ACS APPLIED MATERIALS & INTERFACES

Applications of Polymer, Composite, and Coating Materials

Drying of ethanol/water droplets containing silica nanoparticles

Jing Shi, Lisong Yang, and Colin D. Bain

ACS Appl. Mater. Interfaces, **Just Accepted Manuscript** • DOI: 10.1021/acsami.8b21731 • Publication Date (Web): 22 Mar 2019

ACS Publications

is published by the American Chemical Society. 1155 Sixteenth Street N.W., Washington, DC 20036

Drying of ethanol/water droplets containing silica nanoparticles

*Jing Shi, Lisong Yang, and Colin D. Bain**

Department of Chemistry, Durham University, Durham, DH1 3LE, U.K.

KEYWORDS: inkjet printing, binary droplet, hydrophobic nanoparticles, deposit morphology, Marangoni flow, sol–gel transition.

ABSTRACT: The evaporation of colloidal drop on a substrate with a pinned contact line usually results in a ring stain (the so-called coffee-ring effect). In this paper, we present an investigation of the evaporation of sessile picoliter droplets of binary solvent mixtures containing fumed silica nanoparticles (NPs). The internal flows in ethanol/water droplets are suppressed and uniform deposit morphology achieved with a low loading (0.2–0.5 vol.%) of hydrophobic fumed silica NPs. The effective control of the particle deposit morphology is based on a rapid sol–gel transition assisted by preferential evaporation of ethanol. For droplets of dilute suspensions, the fumed silica NPs tend to agglomerate

and form an elastic network quickly, starting from the region close to the three-phase contact line and below the gas–liquid interface and growing towards the interior of the droplet, as the solvents evaporate and the surface descends. Higher silica particle concentrations, lower ethanol concentrations, and weaker Marangoni flows all contribute to the sol–gel transition and hence to the suppression of the CRE.

INTRODUCTION

When a spilled coffee drop is dried on a surface, a ring stain is normally observed; this is the widely known 'coffee-ring' effect (CRE). The mechanism behind the CRE has been well established – evaporation rate is highest close to the three-phase contact line of a pinned drop which induces internal flow from the interior to the periphery to replenish the lost fluid. Small particles suspended in the drop follow this outward capillary flow and are transported to the contact line where they ultimately deposit and form a ring.[1,2] Suppression of the CRE is of great interest due to the broad applications of inkjet printing from traditional graphics to functional devices.[3-12] Various strategies have been employed to control the CRE: (i) suppression of capillary flow via sol–gel transition;[13-16] (ii) prevention of contact-line pinning via substrate treatment to cause the contact line to retract, negating the outward capillary flow;[17-20] (iii) particle assembly at the gas–liquid interface via rapid evaporation[21,22] and/or adsorption of the particles to the gas–liquid interface through manipulation of particle charge[23], amphiphilicity[24] or shape[25-28]; (iv) enhancement of particle–substrate interactions;[29,30] (v) recirculation of particles at the three-phase contact line via thermal Marangoni flow (induced by the

temperature gradient at the gas–liquid interface arising from evaporation)[31] or solutal Marangoni flow (induced by concentration gradients at the gas–liquid interface arising from preferential evaporation of one component)[7,32-37]; (vi) in-situ generation of particles from emulsions in which the disperse phase is more volatile than the continuous phase.[38]

Among the aforementioned strategies, understanding of the effect of solutal Marangoni flow on suppressing the CRE is far from complete. Many reports infer the drying mechanisms from the final patterns of deposits without accurately characterising the internal flows. Droplets exhibiting solutal Marangoni flow contain at least two components (solvents, solutes or surfactants) whose concentrations need to be tracked within the droplet and which can interact with particles leading to adsorption and self-assembly,[23,39] or particle migration (variously known as diffusiophoresis or chemophoresis).[40,41] The reported effectiveness of Marangoni flow in controlling the CRE is variable. Park and Moon reported formation of uniform deposits upon drying of binary picoliter droplets with a particular particle concentration and attributed this to solutal Marangoni flow.[32] Majumder et al. found uniform deposits were formed when

water drops were evaporated in an environment saturated with ethanol and explained this by recirculating Marangoni flow induced by non-uniform condensation of ethanol at the liquid surface.[33] However, Kim et al. reported that the deposit formed upon the drying of ethanol/water droplet was non-uniform even with the existence of Marangoni eddies; further addition of surfactants and polymers lead to uniform deposits which were attributed to extended Marangoni flows due to addition of surfactants and strong interaction between particles and the substrate due to the presence of polymers.[36] Talbot *et al.* reported that in binary ethanol/water droplets, even with strong recirculating Marangoni flow, the CRE was not well suppressed due to the outward capillary flow at the later stage of the drying process after Marangoni flow ceased. They also reported strong migration of tracer particles towards the centres of the Marangoni cells where the ethanol concentration was the highest.[42,43] and showed that the particles could be fixed at the centre of the droplet by careful control of inter-particle interactions, rather than at the periphery as in the CRE.[15] While one may be able to find specific conditions under which a particular formulation yields a uniform deposit upon drying, we cannot yet predict how an arbitrary formulation will dry. Given that most practical formulations

contain solutes and/or solvent blends, this ignorance is a significant limitation to the development of inkjet printing of functional materials.

The purpose of this paper is not to present a general prescription for the use of Marangoni effects in suppressing the CRE (though we and others are working towards that objective); rather it demonstrates one means of obtaining a uniform deposit notwithstanding the still-unpredictable effects of Marangoni flows. We focus on binary solvent mixtures which generally give unpredictable results but which, under the right conditions, may give uniform deposits. We extend a strategy that we have demonstrated previously for pure water droplets, that is, to use a sol–gel transition in a nanoparticle (NP) suspension to suppress the capillary flows that give rise to the CRE and to control the Marangoni flows. We also take advantage of the fact that the solvent composition provides an additional variable to tune the interactions between the nanoparticles. Specifically, we use hydrophobic fumed-silica NPs – which are commercially available in large quantities at low cost – as the rheology modifier, and ethanol/water as the binary solvent mixture (since it exhibits particularly strong Marangoni effects).

It is well-known that particle-particle attractions between silica NPs are enhanced if the silica surface and the liquid medium differ in their physicochemical properties.[44,45] We hypothesized that hydrophobic fumed-silica NPs in an ethanol/water droplet would form a network as the ethanol evaporates preferentially to leave a progressively more polar solvent. Furthermore, the network would grow below the gas–liquid interface because the particles become more concentrated near the gas–liquid interface as the droplet evaporates. A typical sessile droplet in our experiments has a contact diameter of 200 μm, initial height of 30 μm and a characteristic vertical velocity h/t_{dry} of $O(10)$ μm s^{-1}, where h is droplet height, and t_{dry} the drying time. The diffusion coefficient, D, for fumed silica NPs with a hydrodynamic diameter of a few hundreds of nm is $O(1)$ μm^2 s^{-1}. Consequently, the Peclet number, $Pe = hU/D = O(10^2)$, indicating that convection of NPs dominates over diffusion. Hence as the droplet evaporates the NPs are swept up beneath the receding interface leading to a local concentration near the interface that is much higher than the average concentration in the droplet.

We are not the first to notice the potential of sol–gel transitions in fumed silica NPs to control drying patterns. Anyfantakis et al.[14] explored the drying of microliter drops of

pure water containing fumed silica NPs of varying hydrophobicities. They showed that the deposition patterns were related to the hydrophobicity and the concentration of the fumed silica NPs: the most uniform deposits were formed at moderate to high loadings of hydrophobic fumed silica NPs (0.5 vol.% for particles with 33% surface Si–OH, and 1 vol.% for 51% surface Si–OH). They interpreted their observations in terms of a bulk sol–gel transition, but did not study the rheology in depth. In this paper, we focus our attention on picolitre droplets, which evaporate sufficiently quickly (few seconds) to be useful for practical manufacturing applications. As noted above, we are also interested in solvent blends rather than pure water. We show that fresh hydrophobic fumed silica rapidly forms a 3-dimensional viscoelastic network below the gas–liquid interface of an evaporating ethanol/water droplet, suppressing Marangoni flow and finally leading to a uniform deposit; effective control was obtained with a loading of hydrophobic fumed silica NPs (0.2–0.5 vol.%) that is much lower than in our previous study in which 2–3 wt.% laponite NPs were used to control the deposition of particles in water droplets[13,15]. We also present rheological measurements of the NP suspensions to help us to

understand the interaction between Marangoni stresses and the non-Newtonian rheology of the suspensions.

EXPERIMENTAL SECTION

Sample Preparation. Fumed silica NPs (Wacker Chemie AG) were used as received. The primary structure of fumed silica consists of branched aggregates (100–250 nm in size) formed by the fusion of primary spherical particles (5–30 nm in size), as shown in Figure 1a. Most experiments were conducted with a hydrophobic fumed silica, HDK® H20, which is functionalised with dimethyl silyl groups ($Si–(CH_3)_2$) and has a silanol ($Si–OH$) content of 50% relative to hydrophilic silica. A few experiments were performed with hydrophilic fumed silica NPs (HDK® N20).

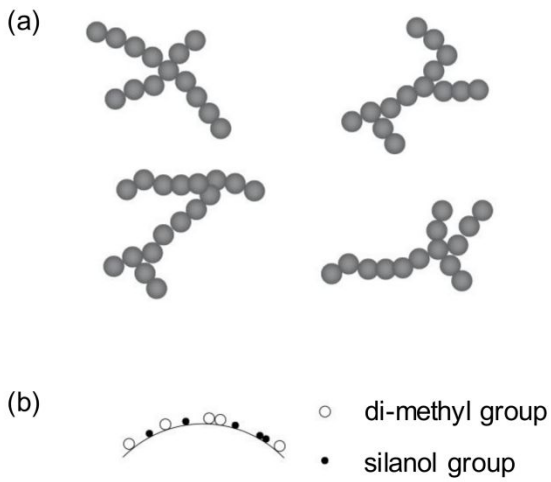

Figure 1. Schematic representation of primary structures of fumed silica (a) and the fumed silica surface (b). The primary structure consists of branched aggregates (100–250 nm in size) formed by the fusion of primary spherical particles (5–30 nm in size).

Ultrapure water (Milli-Q, Merck) and Ethanol (Fisher Scientific, 99.8%) were used as the solvents. To prepare the suspensions of silica NPs in an ethanol/water mixture, suspensions of silica in ethanol were prepared first. The fumed silica NPs were gradually added into ethanol under magnetic stirring and the mixture was sonicated over 30 mins to obtain a homogeneous suspension of silica in ethanol. A stock suspension of 2 vol.% NPs was prepared first; suspensions with lower concentrations of NPs were prepared by diluting the stock suspensions with ethanol. Then water was gradually added into the suspension under magnetic stirring and the mixture was further sonicated for at least 30 mins to obtain the final suspension. For samples used for inkjet printing, 0.01 vol./% polystyrene (PS) particles (median diameter 997 nm, steric stabilized by polyethylene glycol methacrylate (PEGMA)[46]; University of Leeds, U.K.) were added as tracer particles. For inkjet printing the concentrations of fumed silica NPs

was 2.2 – 22 mg/mL, which is 0.1 to 1 vol.% based on an assumed density of the primary particles of 2.2 g cm^{-3}. Suspensions with higher loadings of solid content (0.5–3 vol.%) in ethanol/water mixtures were studied in rheological experiments.

Rheology. An AR 2000 rheometer (TA Instruments) with a cone (60 mm diameter, 2° angle) and plate geometry and a solvent trap cover was used. The rheology of suspensions of silica NPs in pure ethanol and in ethanol/water mixtures, without the inclusion of PS particles, were determined under both steady shear (strain rate $\dot{\gamma}$ = 0.01–1000 s^{-1}) and oscillatory shear (ω = 0.1–100 rad s^{-1}). In steady-shear experiments, the viscosity of a sample is measured as a function of shear rate. In dynamic experiments, a low-amplitude sinusoidal strain, γ, is imposed on the sample at a fixed frequency, ω, and a maximum strain amplitude γ_0: $\gamma = \gamma_0 \sin(\omega t)$. Within the region of linear viscoelasticity, the resulting stress is also sinusoidal, having a phase difference, δ, with the strain. It can be decomposed into an in-phase and an out-of-phase component:

$$\sigma = \sigma_0 \sin(\omega t + \delta) = G' \gamma_0 \sin(\omega t) + G'' \gamma_0 \cos(\omega t)$$

where $G' = \frac{\sigma_0}{\gamma_0}\cos\delta$, and $G'' = \frac{\sigma_0}{\gamma_0}\sin\delta$. The storage modulus G' is related to the elastic energy stored in the system on deformation, and the loss modulus G'' is related to the viscous dissipation of energy in the system. G' is an important indicator of the formation of extended networks of particles that resist deformation in colloidal suspensions.

Printing. The experimental setup used to image the drying process of picoliter droplets is shown in Figure 2. Droplets (450 ±100 pL, contact diameter ~ 200 μm) were ejected from a print head (MJ-ABP-01, Microfab Technologies) with a 50-μm diameter orifice onto a transparent glass substrate (water contact angle = 35 ± 5°). The drying process from side view and bottom view can be recorded simultaneously with two high-speed cameras ('Camera A' and 'Camera B' in Figure 2) upon the triggering of the Microfab driver to dispense a drop. The tracer particles are visible in a dark-field with oblique illumination ('LED C' in Figure 2) from the bottom-view movies. Trajectories of the tracer particles are derived using particle tracking code adapted from open source Matlab routines developed at Georgetown University[47]. Volume profiles of drying droplets are derived from the side-view shadowgraph-movies by a custom-written Matlab code with

an assumption that the droplet is axisymmetric. The resolution of the side and bottom view images is around 0.6 and 0.4 μm/pixel, respectively. The focal planes of the bottom-view movies discussed in this manuscript are at or slightly above the substrates. The printing experiments were conducted in ambient environment with relative humidity, RH = 50 ±10 %.

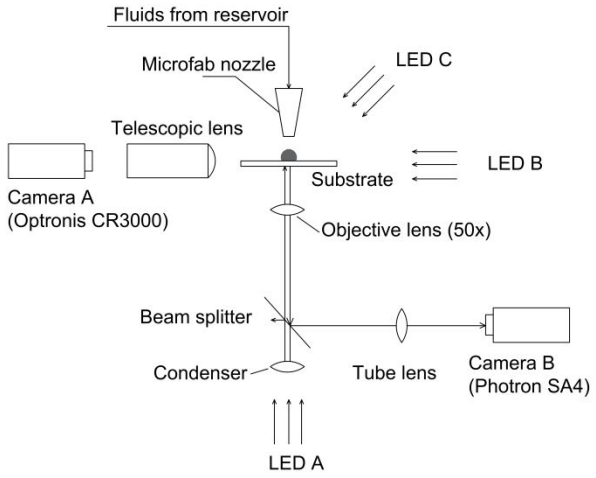

Figure 2. Schematic of the printing rig.

Surface Profilometry. Height profiles of the deposits of pico-litre droplets were measured with a stylus profilometer (KLA Tencor P-6 with a 2 μm stylus). A line scan of 250 μm length across the approximate centre of a deposit was performed; deposits from

several individual droplets obtained under the same experimental conditions were scanned. The lateral resolution of the scans was 0.5 μm/pixel.

Surface Tension. The surface tension of microliter drops of suspensions of silica NPs in an ethanol/water mixture was measured by the drop-shape method (FTÅ 200 tensiometer, First Ten Angstroms). Air bubbles were formed on the tip of a J-shaped capillary immersed in the suspension.

All the experiments were carried out at an ambient temperature of 21±1 °C.

RESULTS AND DISCUSSION

Rheology. Figure 3 shows the steady-shear viscosity of hydrophobic fumed silica NPs in pure ethanol as a control. For a NP concentration ≤ 4 vol.% the suspensions are Newtonian; at higher concentrations they are weakly shear-thinning. The hydrophobic NPs are difficult to disperse in pure water[14] and the rheology was not measured.

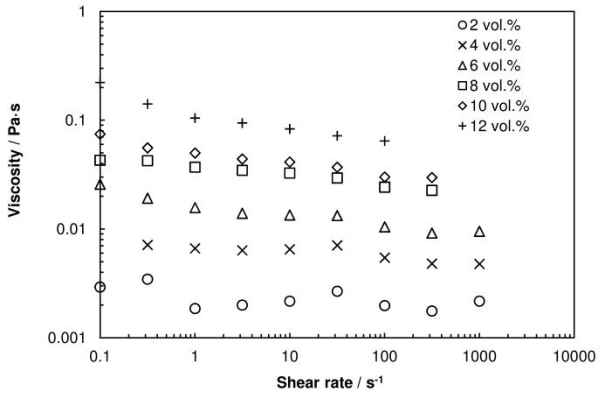

Figure 3. Steady-shear viscosity as a function of shear rate for ethanol containing different concentrations of hydrophobic silica NPs.

The steady-shear rheology of hydrophobic NP suspensions in a 50 vol% ethanol/water mixture (Figure 4a) shows a strong thickening effect of the NPs, which is attributed to dispersion interactions between alkyl chains grafted onto the particle surface.[44,45] The hydrophobic interaction also becomes more important as the water content of the solvent increases. The suspensions with 0.5 and 1 vol.% hydrophobic silica NPs are shear-thinning at $\dot{\gamma} < 1\ s^{-1}$ and Newtonian at higher shear rates. Since the shear rates in a drying droplet are typically $> 1\ s^{-1}$ (see below), these suspensions are expected to show Newtonian behaviour in a drying droplet. For NP concentrations > 1%, the suspensions are shear-thinning over the whole range of shear rates studied

(0.01–1000 s^{-1}) indicating the formation of stronger networks. Visually, the suspensions with 1.2, 1.5 and 2 vol.% silica NPs are viscous sols and the suspension with 3 vol.% silica NPs is a gel (see Figure S1 for pictures of inverted bottles showing that the 3 vol.% sample has a yield stress).

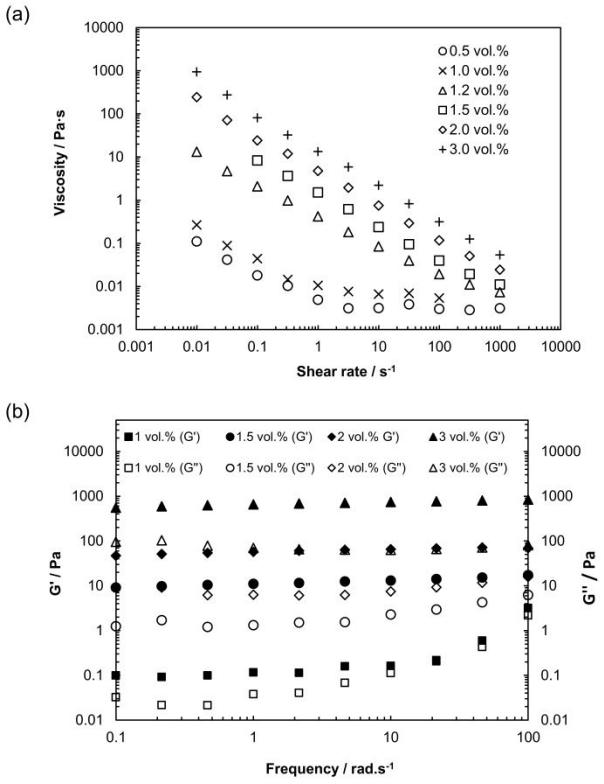

Figure 4. Rheology of 50 vol.% ethanol/water mixtures containing different concentrations of hydrophobic silica NPs.(a) steady-shear viscosity as a function of shear rate; (b) elastic moduli (G') and loss moduli (G'') as a function of frequency from oscillating shear rheology.

The oscillating-shear rheology for particle concentrations between 1 and 3 vol.% is shown in Figure 4b. All suspensions show viscoelastic behaviour. The general picture is of moduli G' and G'' that are independent of frequency and with a storage modulus that is greater than the loss modulus i.e. the response to stress is predominantly elastic. The exception is the lowest concentration of silica NPs (1 vol.%) where both G' and G'' increase with frequency above 10 and 1 rad s^{-1}, respectively. The marked difference in the steady-shear and oscillating-shear rheology suggests that the particle networks are preserved under small deformations (oscillating shear) but disrupted at large strains (steady shear). The strong shear thinning under steady shear then reflects the dynamics of the network formation process. We note that for the 3 vol.% suspension, G' is around 1 kPa, which exceeds the Laplace pressure in the spherical-cap droplets. Thus an increase in the (local) concentration of silica NPs to 3 vol.% is expected to be sufficient to suppress capillary flows in the absence of strong shear. Steady-shear rheology for suspensions of hydrophilic silica NPs in ethanol/water mixtures is shown in Figure S2: hydrophilic silica can be easily dispersed in either ethanol or water and no significant thickening of the suspensions by the hydrophilic NPs was observed.

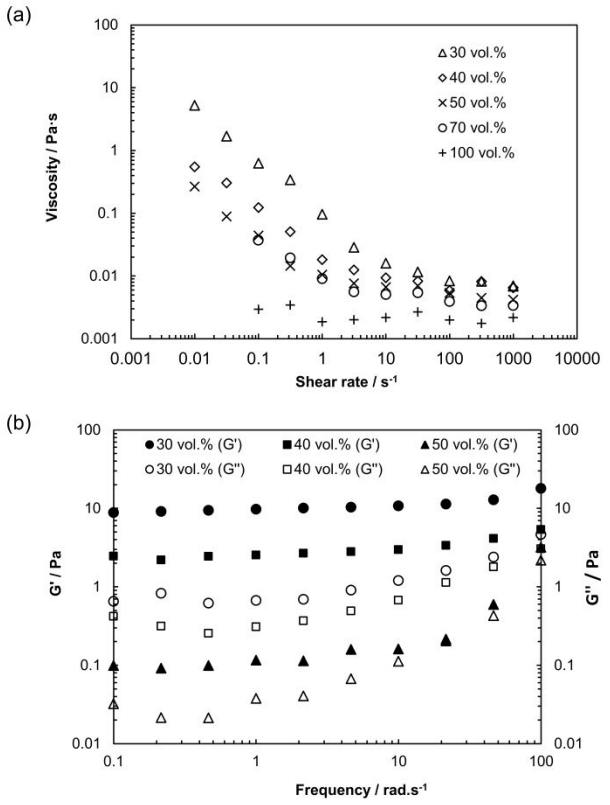

Figure 5. Rheology of ethanol/water mixtures with various ethanol concentrations and 1 vol.% hydrophobic silica NPs. (a) steady-shear viscosity as a function of shear rate; (b) elastic moduli (G') and loss moduli (G'') as a function of frequency from oscillating shear rheology.

Figure 5 shows the influence of ethanol concentration on the rheology of 1 vol.% silica suspensions. Both the steady-shear viscosity and the elastic modulus G' increase as the concentration of ethanol in the binary solvent decreases. As the water content increases

in the binary solvent, particle–particle interactions are enhanced through hydrophobic interactions. The Peclet number for diffusion of the solvent in the evaporating droplets is O(1) so appreciable concentration gradients develop as ethanol evaporates preferentially from the surface. The surface region is depleted in ethanol which, according to the data in Figure 5, should enhance the elasticity of the fluid. For the 10 and 20 vol.% ethanol/water mixture containing 1 vol.% silica NPs, the measured viscosity is lower than that in 30 vol.% ethanol/water mixture (see Figure S3), but these solutions are not homogeneous. The suspensions of silica NPs in ethanol/water mixture were prepared by gradually adding water to suspensions of silica NPs in pure ethanol under magnetic stirring. As water was added to the suspension, the suspension became increasingly viscous or even a gel until further addition of water led to the break-up of the suspension into globules which persisted for an extended time; the continuous phase was depleted in NPs leading to a decrease in the viscosity of the multiphase mixture.

The strong shear-thinning behaviour of suspensions of silica NPs in ethanol/water allows the fluids to be jetted from an ink-jet print head, where the shear rate is of the

order of 10^5 s^{-1}. Once on the substrate, the shear rates inside the sessile droplets are much lower. Neglecting Marangoni flows, the shear rates in the initial stage of the drying can be estimated from U_r/h = O(1) s^{-1} (where U_r is the characteristic radial velocity, ~10^{-4} m s^{-1}). When recirculating Marangoni flows exist, the recirculating flows lead to much larger shear rates given by $2U_r/h$ = O(100) s^{-1} (where U_r is the maximum radial velocity). As the droplets evaporate, the elastic modulus G' increases near the gas–liquid interface due both to the sweeping effect of the receding surface and the reduction in the local concentration of ethanol. Once G' exceeds the Laplace pressure, $p = 2\sigma/r_c$, (where σ is the surface tension and r_c the radius of curvature of the droplet) the effect of the sol–gel transition should be observable as a decrease in capillary flows and a deviation in the drop profile from a spherical cap. For a 50 vol. % ethanol/water suspension with surface tension σ = 27 mN m^{-1}, h = 15 μm (the droplet height at ~ 0.2 t_{dry}) and contact radius, R = 100 μm, the Laplace pressure p = 158 Pa. Therefore, once G is O(10^2) Pa (at low strains – see below) we expect to suppress convective transport within the droplet. From Figure 4b, this elasticity is achieved for 2 vol.% silica NPs in 50

vol.% ethanol/water, and at lower NP concentrations as the ethanol concentration decreases.

Drying of Droplets: Influence of Particle Surface Chemistry. Figure 6 shows the drying of ethanol/water droplets containing 0.2 vol.% hydrophilic and hydrophobic NPs (dark field view: the bright dots are the tracer particles that scatter light). The movies of the drying droplets are provided as supporting information (Movies S1 and S2). For picoliter ethanol/water droplets without any silica NPs, Talbot *et al.* reported that the tracer particles recirculate and migrate towards the centre of the droplet. Before all the ethanol has evaporated, the Marangoni recirculation ceases and is replaced by evaporation-driven capillary flow, leading to a ring stain.[15,42,43] For ethanol/water droplets containing hydrophilic NPs, the tracer particles reveal similar internal flows (Figure 6a and Movie S1). For ethanol/water droplets containing hydrophobic silica NPs (Figure 6b), Marangoni flow was initially observed but rapidly died away. Figure 7 shows the trajectories of the tracer particles during the drying process illustrated in Figure 6b. Particles near the three-phase contact line were fixed first (~0.15 t_{dry}), and particles in the central part of the droplet ceased moving later (~0.35 t_{dry}). The final distribution of

particles (NPs + tracers) in the dry deposit (right-hand images in Figure 6) is even for the hydrophobic NPs, and non-uniform with a pronounced ring stain for the hydrophilic NPs. From the rheology of the formulation and the characteristics of the drying process, we infer that a network of silica NPs is formed early in drying, starting near the three-phase contact line and below the gas–liquid interface, and growing towards the interior of the droplet. We note that the capillary number, $Ca = U_r \mu / \sigma$ (where μ is the shear viscosity) is << 1 for $\dot{\gamma}$ > 1 s^{-1}, so elasticity plays a more important role than viscosity in suppressing capillary flows.

The scattering from the drying droplets is at its brightest shortly before the droplet is finally dry (Figure 6(a)(iv) and 6(b)(iv)) which is unusual since the refractive index contrast between silica and water is less than between silica and air. We interpret this observation as the formation of micro-structures of agglomerated silica NPs that are large enough and dense enough to scatter light. Once the droplet finally dries, these structures coalesce into a continuous film that modifies the reflectivity of the substrate but does not scatter light strongly. In the dry deposits, the observed scattering is mostly from the PS tracer particles.

The SEM images of the dry deposits are shown in Figure 8. The CRE is effectively suppressed in the ethanol/water droplet containing hydrophobic silica NPs, though there remains some internal structure in the dry deposit on the micron length-scale.

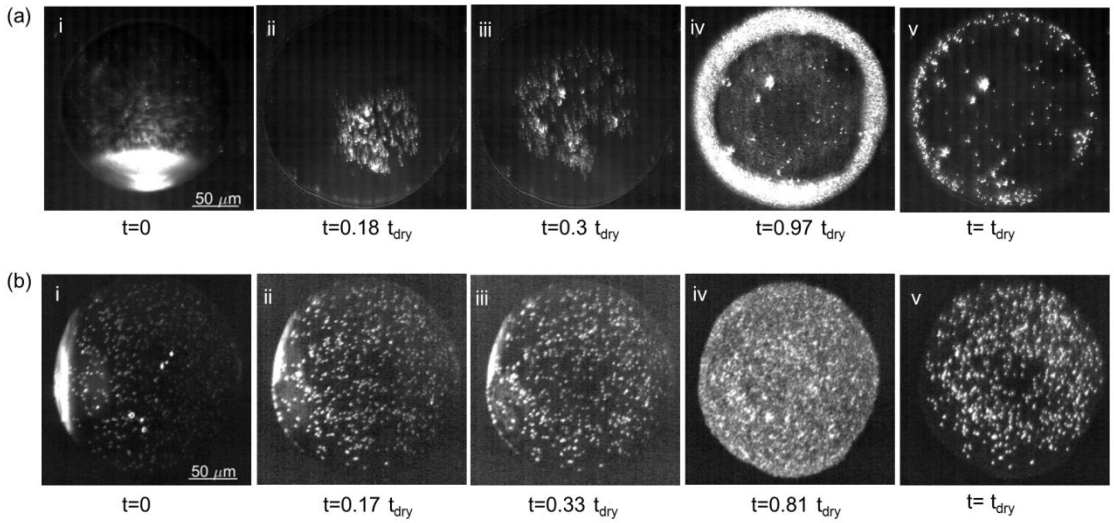

Figure 6. Dark-field images of a drying 50 vol.% ethanol/water droplet with 0.2 vol. % hydrophilic silica particles (a, t_{dry} = 4.6 s), and 0.2 vol.% hydrophobic silica particles (b, t_{dry} = 2.3 s). Both systems contain 0.01 vol.% PS tracer particles.

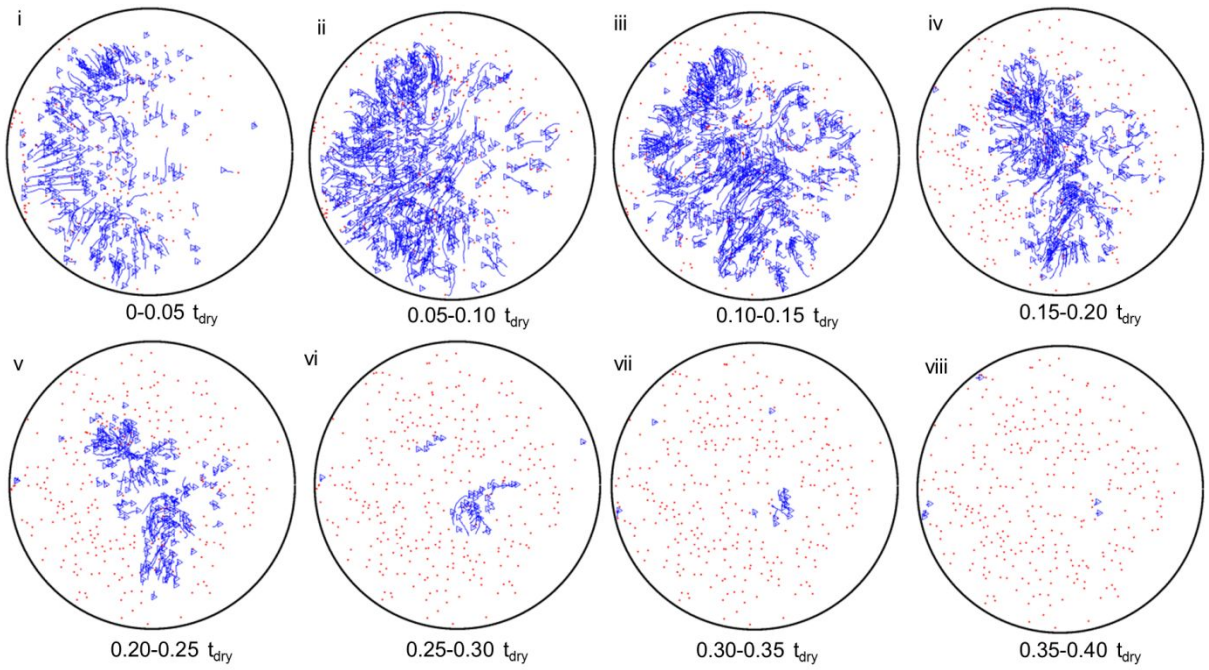

Figure 7. Tracer particle trajectories of a drying 50 vol.% ethanol/water droplet with 0.2 vol. % hydrophobic silica particles and 0.01 vol.% PS tracer particles. Refer to Figure 6b for the dark field images of the drying process. The red dots represent the stationary particles in the radial direction (movement < three pixels in the time interval). The blue lines represent the trajectories of moving particles, having a triangle at the end of the track to show the direction of motion.

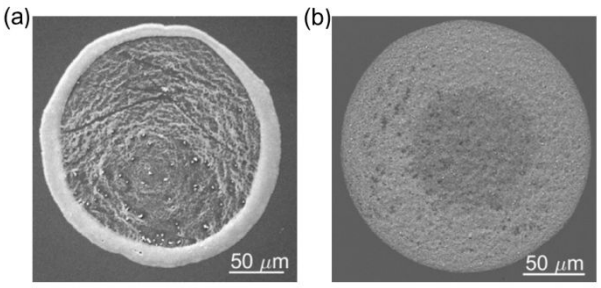

Figure 8. SEM images of deposits upon drying of a 50 vol.% ethanol/water droplet with 0.2 vol. % hydrophilic silica (a), and 0.2 vol.% hydrophobic silica (b). Both systems contain 0.01 vol.% PS tracer particles.

The side view images corresponding to the bottom-view images in Figure 6b are shown in Figure 9. The volume profile, $V(t)$, extracted from the side view images is plotted in Figure 10. The droplet shape deviated from a spherical cap from ~0.17 $_{dry}$, which indicates formation of a gel with a yield stress greater than the capillary pressure. Gelation at the gas–liquid interface suppresses Marangoni flows throughout most of the droplet within the first quarter of the drying time. By this point, the half the volume still remains and the core of the droplet, remote from the gas–liquid interface, still contains a high volume fraction of ethanol and a low concentration of silica NPs – the large Peclet number means that the NPs do not diffuse from the surface towards the substrate.

Consequently the core of the droplet will still be liquid so we might still expect to see tracer particles away from the free surface being transported to the contact line. The driving force for the capillary flows that lead to the CRE, however, arises from the minimisation of the free surface area with a pinned contact line, which preserves the spherical cap. Figure 9 shows that the droplet deviates from a spherical cap early in drying and flattens in the centre; the enhanced curvature near the contact line compared to the apex would lead to a Laplace pressure gradient driving a flow in the opposite direction (away from the contact line). For comparison, the side view images corresponding to the bottom-view images in Figure 6a are shown in Figure S5. No deviation from spherical caps was observed.

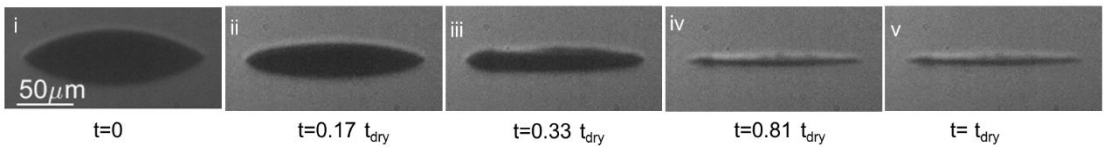

Figure 9. Side-view shadowgraph images of a drying 50 vol.% ethanol/water droplet with 0.2 vol.% hydrophobic silica particles and 0.01 vol.% PS tracer particles.

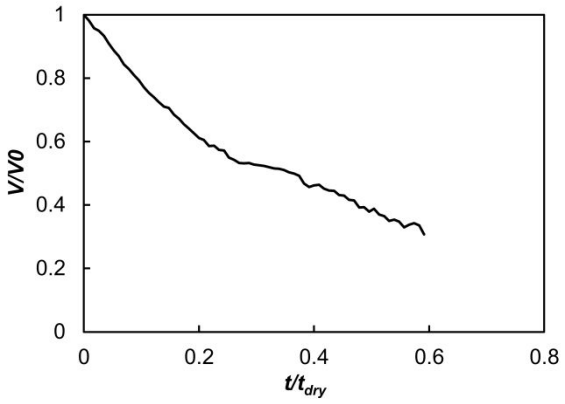

Figure 10. Volume profile with time for a drying 50 vol.% ethanol/water droplet with 0.2 vol.% hydrophobic silica particles and 0.01 vol.% PS tracer particles.

The data presented above were acquired with a fresh batch of hydrophobic fumed silica. We observed that as the hydrophobic fumed silica aged, it became less effective in suppressing the CRE. Figure S6 compares dry deposits with fresh silica and eight months after opening the container. Suppression of the internal flows for aged silica NPs occurred later than with fresh silica NPs; the shape of the droplets observed from side-views was also more like a spherical cap, which leads to internal capillary flows in the fluid region within the bulk of the droplet. While the deposit was still uniform in the centre of the deposit, a build-up of nanoparticles at the contact line was also observed. The bulk rheology of the hydrophobic silica NPs also changed with time (Figure S7). In

the ‘aged’ sample, a 3 vol.% suspension is a running gel, compared to the fresh sample of the same concentration that shows a yield stress sufficient to support its own weight. Thus the interparticle interactions in the aged sample are weaker than in the fresh sample. The origin of the ageing is unknown but could be from adsorption of atmospheric contaminants onto the particle surface or to hydrolysis of the dimethylsilyl groups by atmospheric moisture.

Drying of Droplets: Influence of NP Concentration. Typical morphologies of deposits and height profiles for ethanol/water droplets with different concentrations of hydrophobic silica NPs are shown in Figure 11. At a low silica NP concentration of 0.1 vol.%, wide ring stains were observed (Figure 11 (i)). As the silica NP concentration increased, pancake-shaped deposits with relatively homogenous height profiles were formed (Figure 11 (ii)–(iv)). In Figure 11b (ii) and (iii) the average film height due to the NPs is below 1 μm, so the tracer particles (median diameter 1 μm) protrude above the film. For the lowest concentration, the initial silica NP concentration of a droplet is too low to form an elastic network strong enough to resist the capillary flows towards the contact line, leading to ring stain in Figure 11a(i). The 0.1 vol.% silica NP suspensions

would sometimes depin during drying (Figure S8), while the higher concentrations, which rapidly gelled near the contact line, never depinned. When the initial silica NP concentration of a droplet was ≥ 0.2 vol.%, the surface of the droplet rapidly gelled and relatively uniform deposits were formed independent of the concentration. We note that the higher concentrations had a tendency to gel in the nozzle and inhibit printing of the droplet.

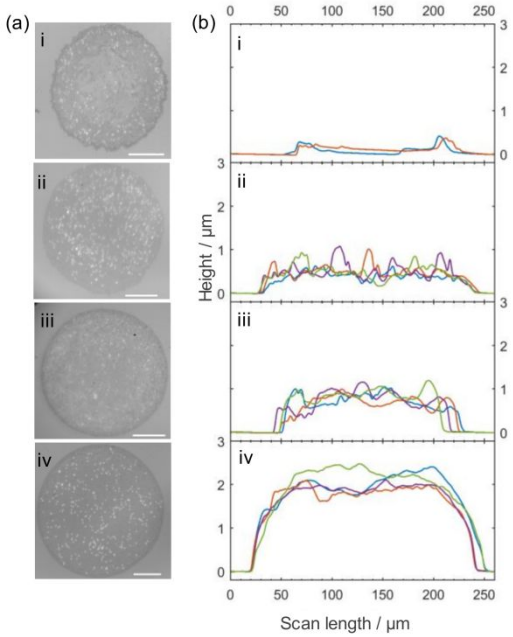

Figure 11. Reflection bright-field microscope images (a) and height profiles (b) of deposits upon drying of 50 vol.% ethanol/water droplets containing different concentrations of hydrophobic silica NPs: (i) 0.1 vol.%, (ii) 0.2 vol.%, (iii) 0.5 vol.%, (iv) 1

vol.%. All samples contained 0.01 vol.% PS tracer particles. The scale bars are 50 μm. Different coloured line profiles were measured from separate droplets dried under the same conditions.

To explore whether the adsorption of the hydrophobic silica NPs at the gas–liquid interface also plays a role in the formation of a gel and the suppression of Marangoni flows, we measured the static interfacial tensions between air bubbles and suspensions with different silica NP concentrations (0–1 vol.%) in a 50 vol. % ethanol/water mixture (see Figure S9). The interfacial tensions of the NP suspensions were within 0.3 mN m^{-1} of that of the pure solvent, providing no evidence for adsorption of silica NPs on the interface. Ellipsometric measurements (see Supplementary Information) also provide no support for significant adsorption of silica NP networks at the surface of ethanol/water mixtures. Therefore, we deduce that the suppression of Marangoni effects is due to a sol–gel transition in NP networks below the gas–liquid surface and not the thermodynamic adsorption of NPs to the gas–liquid surface.

The average thickness, $\bar{h}$, of the NP deposits formed from droplets containing 0.2, 0.5 and 1.0 vol.% silica are around 480, 740 and 2030 nm, respectively (Figure 11b(ii)–(iv)). The volume fraction, ϕ, of the solid within the dry film is given by $\phi = \frac{V_0 C_s}{\pi R^2 \bar{h}}$, where V_0 is the droplet volume, and C_s the particle concentration by volume in the formulation. For the deposits of droplets containing 0.2–1 vol.% silica NPs, the solid concentration in the final deposits was 6–15 vol.%. The specified bulk density of the silica powders is 30–100 kg/m^3, equivalent to 1–5 vol.%, reflecting the open nature of the aggregates. Therefore the dry deposits are highly porous, but denser than the silica powders as received. The porous nature of the deposits is clear in SEM images taken under high magnification (Figure S10).

Drying of Droplets: Influence of Ethanol Concentrations. Figure 12 displays images during the drying process for 0.2 vol. % hydrophobic silica NPs in ethanol/water mixtures with ethanol concentrations of 10 vol. % and 30 vol.% (see also Movies S3 and S4). Refer to Figure 6b for droplets of 50 vol.% ethanol/water for comparison. The bright scattering from the 10 vol.% ethanol suspension at early times suggests that the

suspension is inhomogeneous as noted above in the rheology section. The trajectories of the tracer particles during drying are shown in Figure 13. As the elastic modulus is higher for a suspension with a lower ethanol concentration in the binary solvent, one might expect an earlier sol–gel transition during drying for droplets with lower ethanol concentrations. The real drying process is more complex. The formation of a gel is a competition between the elasticity of the viscoelastic network and the shear stresses caused by the internal flows. Higher shear rates cause shear thinning and inhibit the formation of a gel if the rate of gelation is slow compared to the shear rate. Talbot reported that the Marangoni flow in an ethanol/water droplet without any fumed silica NPs is strongest when the initial ethanol concentration is around 30 vol.%; the shear rate in the early stage of drying of a 30 vol.% ethanol/water droplet is nearly one order of magnitude higher than that of a 50 vol.% ethanol/water droplet (see Fig. 4.10 in Ref 48), while the shear rate in a 10 vol. % mixture is about 3 times larger than in the 50 vol.% droplet.[48]

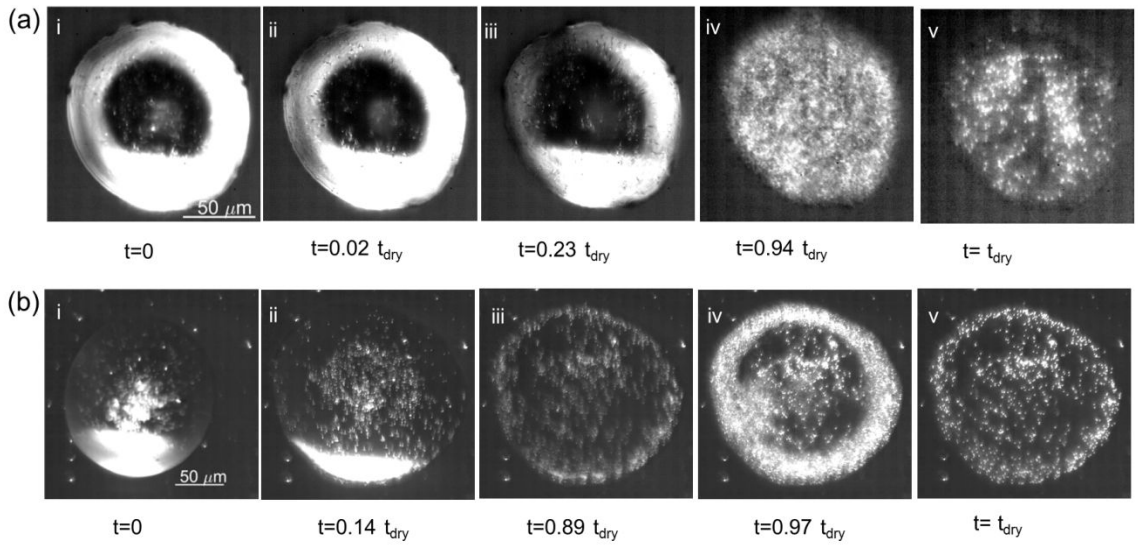

Figure 12. Dark-field images of a drying ethanol/water droplet with 0.2 vol.% hydrophobic silica particles and 0.01 vol.% PS tracer particles. (a) 10 vol.% ethanol/water; (b) 30 vol.% ethanol/water.

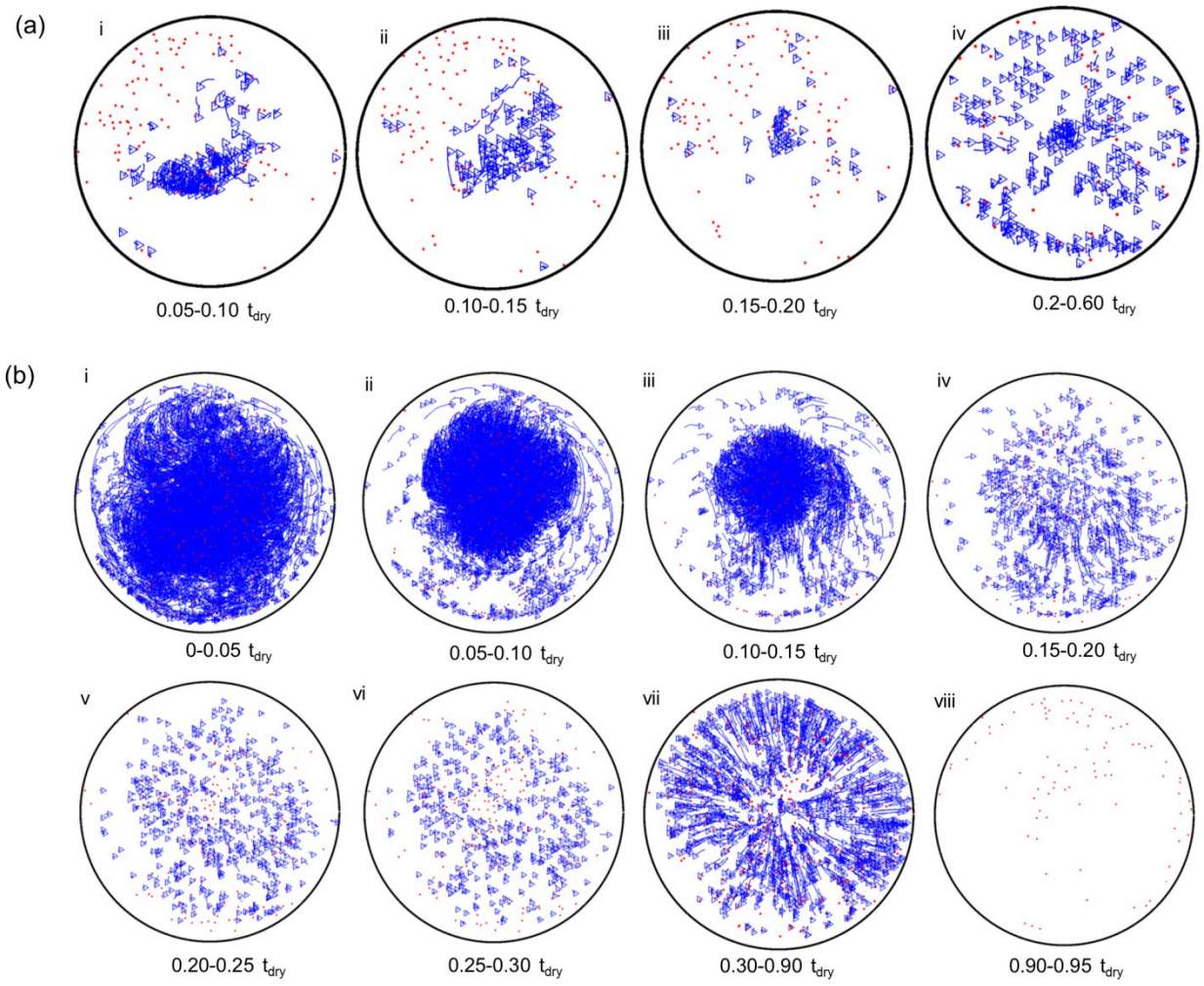

Figure 13. Particle trajectories of a drying ethanol/water droplet (a-10 vol.% ethanol/water; b-30 vol.% ethanol/water) with 0.2 vol. % hydrophobic silica particles and 0.01 vol.% PS tracer particles. Refer to Figure 12 for the dark field images of the drying process. The red dots represent the stationary particles in the radial direction (movement < three pixels in the time interval). The blue lines represent the trajectories

of moving particles, having a triangle at the end of the track to show the direction of motion.

The data for 0.2 vol.% hydrophobic NPs in 10 vol.% ethanol (Figure 13a) and 50 vol.% ethanol (Figure 7) show that the sol–gel transition occurs earlier in the former case. Movement of tracer particles ceased near the contact line by 0.05 $t_{dry,}$ and virtually all the particles had stopped moving by 0.2 $t_{dry.}$ Over the remainder of the drying period there is a small inward movement of the particles. As noted above, a very bright field was observed just before complete drying of the droplet (Figure 12a(iv)). The final deposits had an even distribution of particles (Figure 12a(v) and Figure 14(i)). In 10 vol.% ethanol, the stronger interparticle interactions compared to 50 vol.% ethanol more than compensate for the higher shear forces, and gelation occurs earlier in the drying process.

The 30 vol.% ethanol/water droplet behaves quite differently (Figure 12b and Figure 13b). The tracer particles recirculate rapidly along the Marangoni streamlines and migrate slowly across the streamlines (the mechanism will be discussed elsewhere) and

collect in a disc in the central part of the droplet (Figures 12b(ii) and 13b(iii)). Comparative data on the drying of a 30 vol.% ethanol/water droplet without any fumed silica NPs is presented in Movie S5 and Figure S9 in the Supporting Information. The hydrophobic silica NPs did not fully suppress Marangoni flow but reduced the duration – the recirculating flow ceased earlier (~0.15 t_{dry} for the case with hydrophobic silica NPs as shown in Figure 13, and around ~0.25 t_{dry} for the case without hydrophobic silica NPs, as shown in Figure S11). After the Marangoni flow ceased, some of the tracer particles remained stationary while others were transported slowly towards the three-phase contact line by capillary flow (between Figure 13b(iv)–(vii)). Movie S4 shows that the stationary particles became brighter as the drop dried, consistent with stationary particles near the free surface moving into the focal plane of the objective lens at the substrate. While the near-surface region had gelled, the bulk of the droplet remained fluid. The dry deposit consists of a central disk from the trapped particles and a ring at the contact line, with an annular region in-between that is depleted of particles. This pattern is seen both for the micron-sized tracer particles (optical images in Figure 12b(iv)) and the silica NPs (SEM and profilometer traces in Figure 14(ii)), implying that

the NPs also show the cross-stream migration in the Marangoni flows and form a central disc similar to the tracer particles. It is not clear why the capillary flows persist after the surface gels in the 30% ethanol solution when they are suppressed in the 10% and 50% ethanol solutions. A higher concentration of silica NPs (0.5 vol.%) does effectively suppress the Marangoni flows in 30 vol.% ethanol/water droplets (Movie S6). The dry deposit appears uniform in microscopic images, but the profilometer shows that the centre is slightly depressed compared to the edges of the drop (see Figure S12).

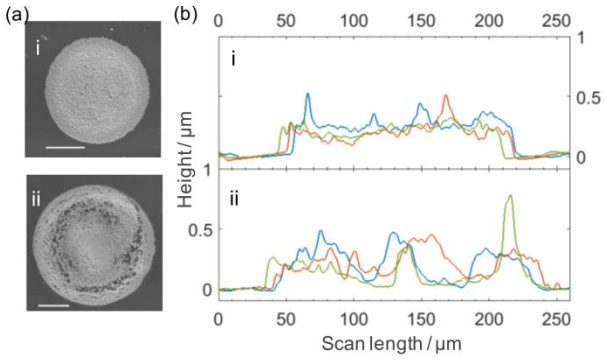

Figure 14. SEM images (a) and height profiles (b) of deposits upon drying of (i) 10 vol.% and (ii) 30 vol.% ethanol/water droplets containing 0.2 vol.% hydrophobic silica NPs and 0.01 vol.% PS tracer particles. The scale bars are 50 µm. Different coloured line profiles were measured from separate droplets dried under the same conditions.

DISCUSSION

Previous studies have shown that the adsorption of particles to the gas–liquid interface to form an elastic 'skin' was an effective mechanism for suppressing the coffee-ring effect.[16,21-26] Our initial hypothesis was that the changing solvent quality as the ethanol evaporates preferentially in ethanol/water mixtures would drive silica nanoparticles to the gas–liquid interface. We observed experimentally that a low concentration (0.2 vol.%) of silica NPs did suppress the Marangoni effects in drying ethanol/water droplets and lead to uniform deposits. Surface tensiometry and ellipsometry measurements did not, however, provide evidence for silica NP adsorption. Rheological measurements on silica NP suspensions showed a sol–gel transition and a yield stress around 3 vol.% of solids which, together with the large Peclet number in the drying droplets, suggests an alternative explanation (see Figure 15). We propose that as the droplet evaporates the receding gas–liquid interface sweeps up the NPs until the near-surface concentration of NPs exceeds the gelation concentration. The sol–gel transition happens first near the contact line where evaporation is fastest, initially

restricting Marangoni flows to the central part of the droplet. Within the first quarter of the drying time, the whole surface gels and Marangoni flows cease throughout the droplet. This process is accelerated by the increasing volume fraction of water near the free surface, which strengthens the networks between the hydrophobic silica particles through hydrophobic interactions. While the core of the droplet may remain liquid, the elasticity of the shell is sufficiently high that the droplet deviates from a spherical cap and the capillary flows towards the contact line that give rise to the CRE are suppressed. The concentration of silica NPs required to yield a uniform deposit in a 50 vol.% ethanol/water mixture is an order of magnitude lower than in our previous work on the sol–gel transitions in aqueous laponite suspensions, which is beneficial for practical applications. Lowering the NP concentration further to 0.1 vol.% did not lead to an obvious sol–gel transition; Marangoni flows followed by outward capillary flows led to a ring stain (Figure 15a).

Obtaining a uniform deposit from particles that are dispersed throughout the bulk rather than adsorbed at the surface requires a subtle balance of gelation and flow. If internal flow is completely suppressed, then the initial distribution of particles in the

sessile drop is projected onto the surface, giving rise to a dome-shaped deposit. Uncontrolled convection, on the other hand, leads to the well-known ring stain. Timing of the gelation is thus important to obtain the most uniform deposit. Density measurements and high resolution SEM images show that the final NP film is highly porous (ϕ = 0.06–0.15). The small primary silica particles (~10 nm diameter) are irreversibly aggregated into three-dimensional structures around 100 nm across. It is the secondary flocculation of these aggregates that leads to an elastic network and the sol–gel transition. The very open structure of the flocs is the reason for gelation at low volume fractions of nanoparticles.

Experiments on the drying of 30 vol.% ethanol/water droplets illustrate some of the complexities of the drying process. This composition shows particularly strong Marangoni recirculation with shear rates, $\dot{\gamma}$, of O(10^3) s^{-1}. The silica NP suspensions are strongly shear-thinning under large strains and the strong Marangoni flows hinder the reformation of the NP networks. Typically one would seek to compare the shear rate with the inverse of the relaxation rate of the network, where the latter is inferred from the cross-over in G' and G'' in oscillating shear experiments. The dynamic rheology

measurements do not, however, show a strong frequency dependence in the elastic and loss moduli, suggesting that the NP networks are retained under strains of small amplitude but broken down under continuous shear. We can only infer therefore that the relaxation time of the network is long on the timescale of the Marangoni flows ($\dot{\gamma}^{-1}$). The 30 vol.% ethanol experiments also show cross-stream migration of particles that concentrates the tracer particles in a disc near the centre of the droplet. While we cannot track individual NPs, the SEM images of the final deposits show a central disk as well as a peripheral ring, consistent with the NPs also migrating into a central disk during Marangoni flows (Figure 15d). Increasing the concentration of hydrophobic silica NPs to 0.5 vol.% was sufficient to suppress the Marangoni flows early in the drying and give a more uniform deposit.

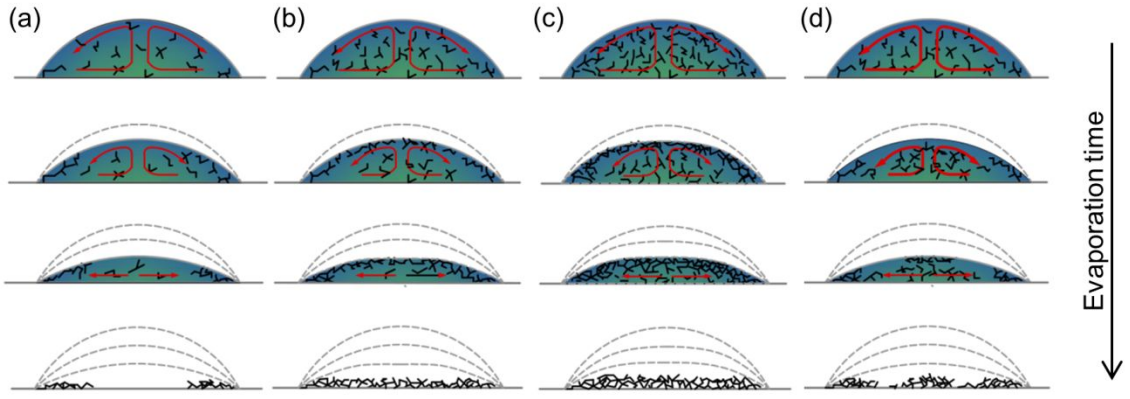

Figure 15. Illustrations of different drying patterns for ethanol/water droplets containing hydrophobic fumed silica. (a) – (c) are for drying of droplets in which Marangoni flow is moderate and (a) low silica concentration (0.1 vol%) where a sol–gel transition does not occur until late in the drying process, (b) medium silica concentration (0.2 vol%), (c) high silica concentration (0.5–1 vol%); (d) is for droplets with medium silica concentration in the presence of strong Marangoni flow (30 vol.% ethanol).

CONCLUSIONS

Solutal Marangoni flows have been proposed to aid the formation of a uniform deposit in the drying of droplets of colloidal suspensions. In binary solvent mixtures, where one component is more volatile than the other, pattern formation in the deposit is a complex process involving both cross-stream migration during the early stages of drying and strong outward capillary flows during the late stage of drying after Marangoni recirculation has ceased. A common consequence is a non-uniform deposit with a ring-stain and/or accumulation of particles in the centre of the deposit. In this paper, we have demonstrated a means to suppress the coffee-ring effect in the drying of binary solvent

droplets via rapid sol–gel transition. The local sol–gel transition in picoliter droplets of ethanol/water mixtures containing a low concentration of fresh hydrophobic fumed silica NPs (0.2–0.5 vol.%) suppresses internal flows and leads to uniform deposits. As the droplet evaporates, the fumed silica particles agglomerate to form a 3D elastic network. The yield stress of this network suppresses Marangoni flows. Gelation starts at close to the periphery where evaporation is fastest and near the gas–liquid interface as the descending surface sweeps up the silica NPs. The network below the gas–liquid interface extends towards the interior of the droplet as evaporation proceeds. Evaporation of ethanol to leave a water-rich layer near the free surface enhances the hydrophobic interactions between the NPs leading to a stronger gel. For droplet compositions with particularly vigorous internal Marangoni convection, a higher concentration of silica NPs is needed to overcome the shear-thinning properties of the suspension.

ASSOCIATED CONTENT

Supporting Information

The following files are available free of charge via the Internet at http://pubs.acs.org.

Additional figures and Ellipsometry Measurements (PDF).

Movie S1 (AVI) – the drying process for a 50 vol.% ethanol/water droplet with 0.2 vol.% hydrophilic fumed silica PSs and 0.01 vol.% PS tracer particles; playback rate 0.05xReal time.

Movie S2 (AVI) – the drying process for a 50 vol.% ethanol/water droplet with 0.2 vol.% hydrophobic fumed silica PSs and 0.01 vol.% PS tracer particles; playback rate 0.05xReal time.

Movie S3 (AVI) – the drying process for a 10 vol.% ethanol/water droplet with 0.2 vol.% hydrophobic fumed silica PSs and 0.01 vol.% PS tracer particles; playback rate 0.05xReal time.

Movie S4 (AVI) – the drying process for a 30 vol.% ethanol/water droplet with 0.2 vol.% hydrophobic fumed silica PSs and 0.01 vol.% PS tracer particles; playback rate 0.05xReal time.

Movie S5 (AVI) – the drying process for a 30 vol.% ethanol/water droplet with 0.005 vol.% PS tracer particles; playback rate 0.05xReal time.

Movie S6 (AVI) – the drying process for a 30 vol.% ethanol/water droplet with 0.5 vol.% hydrophobic fumed silica PSs and 0.01 vol.% PS tracer particles; playback rate 0.05xReal time.

AUTHOR INFORMATION

Corresponding Author

*E-mail: c.d.bain@durham.ac.uk

Notes

The authors declare no competing financial interest.

ACKNOWLEDGMENT

The authors are grateful to Wacker Chemie AG for providing free samples of fumed silica particles, Aixa Pineiro-Romero and Yilin Wang for their help in SEM imaging, and Stephen Boothroyd and Richard Thompson for discussions on rheology results. This work was funded by EPSRC under Grant EP/N025245/1.

REFERENCES

(1) Deegan, R.D.; Bakajin, O.; Dupont, T.F.; Huber, G.; Nagel, S.R.; Witten, T.A. Capillary Flow as the Cause of Ring Stains from Dried Liquid Drops. *Nature* **1997**, 389, 827-829.

(2) Deegan, R.D.; Bakajin, O.; Dupont, T.F.; Huber, G.; Nagel, S.R.; Witten, T.A. Contact Line Deposits in an Evaporating Drop. *Phys. Rev. E* **2000**, 62, 756-765.

(3) Bharathan, J.; Yang, Y. Polymer Electroluminescent Devices Processed by Inkjet Printing: I. Polymer Light-Emitting Logo. *Appl. Phys. Lett.* **1998**, 72, 2660-2662.

(4) Sirringhaus, H.; Kawase, T.; Friend, R.; Shimoda, T.; Inbasekaran, M.; Wu, W.; Woo, E. High-resolution Inkjet Printing of All-Polymer Transistor Circuits. *Science* **2000**, 290, 2123-2126.

(5) de Gans, B.J.; Duineveld, P.C.; Schubert, U.S. Inkjet Printing of Polymers: State of the Art and Future Developments. *Adv. Mater.* **2004**, 16, 203-213.

(6) Aernouts, T.; Aleksandrov, T.; Girotto, C.; Genoe, J.; Poortmans, J. Polymer Based Organic Solar Cells Using Ink-Jet Printed Active Layers. *Appl. Phys. Lett.* **2008**, 92, 033306.

(7) Lim, J.A.; Lee, W.H.; Lee, H.S.; Lee, J.H.; Park, Y.D.; Cho, K. Self-Organization of Ink-jet-Printed Triisopropylsilylethynyl Pentacene via Evaporation-Induced Flows in a Drying Droplet. *Adv. Funct. Mater.* **2008**, 18, 229-234.

(8) Kim, H.; Ge, J.; Kim, J.; Choi, S.-E.; Lee, H.; Lee; Park, W.; Yin, Y.; Kwon, S. Structural Colour Printing Using a Magnetically Tunable and Lithographically Fixable Photonic Crystal. *Nat. Photonics* **2009**, 3, 534-540.

(9) Komuro, N.; Takaki, S.; Suzuki, K.; Citterio, D. Inkjet Printed (bio) Chemical Sensing Devices. *Anal. Bioanal. Chem.* **2013**, 405, 5785-5805.

(10) Jung, S.; Sou, A.; Banger, K.; Ko, D.H.; Chow, P.C.; McNeill, C.R.; Sirringhaus, H. All-Inkjet-Printed, All-Air-Processed Solar Cells. *Adv. Energy Mater.* **2014**, 4, 1400432.

(11) Gillen, G.; Najarro, M.; Wight, S.; Walker, M.; Verkouteren, J.; Windsor, E.; Barr, T.; Staymates, M.; Urbas, A. Particle Fabrication Using Inkjet Printing onto Hydrophobic Surfaces for Optimization and Calibration of Trace Contraband Detection Sensors. *Sensors* **2015**, 15, 29618-29634.

(12) Parry, A.V.; Straub, A.J.; Villar-Alvarez, E.M.; Phuengphol, T.; Nicoll, J.E.; Jordan, L.M.; Moore, K.L.; Taboada, P.; Yeates, S.G.; Edmondson, S. Submicron Patterning of Polymer Brushes: An Unexpected Discovery from Inkjet Printing of Polyelectrolyte Macroinitiators. *J. Am. Chem. Soc.* **2016**, 138, 9009-9012.

(13) Talbot, E.L.; Yang, L.; Berson, A.; Bain, C.D. Control of the Particle Distribution in Inkjet Printing through an Evaporation-Driven Sol–Gel Transition. *ACS Appl. Mater. Interfaces* **2014**, 6, 9572-9583.

(14) Anyfantakis, M.; D. Baigl; B.P. Binks. Evaporation of drops containing silica nanoparticles of varying hydrophobicities: Exploiting particle–particle interactions for additive-free tunable deposit morphology. *Langmuir* 2017, **33,** 5025-5036.

(15) Talbot, E.L.; Yow, H.N.; Yang, L.; Berson, A.; Biggs, S.R.; Bain, C.D. Printing Small Dots from Large Drops. *ACS Appl. Mater. Interfaces* **2015**, 7, 3782-3790.

(16) Mayarani, M.;. Basavaraj, M.G; Satapathy, D.K. Viscoelastic Particle Laden Interface Inhibits Coffee-Ring Formation. *Langmuir* **2018**, 34, 14294-14301

(17) De Gans, B.-J.; Schubert, U.S. Inkjet Printing of Well-Defined Polymer Dots and Arrays. *Langmuir* **2004**, 20, 7789-7793.

(18) Ko, H.-Y.; Park, J.; Shin, H.; Moon, J. Rapid Self-Assembly of Monodisperse Colloidal Spheres in an Ink-Jet Printed Droplet. *Chem. Mater.* **2004**, 16, 4212-4215.

(19) Yang, Q.; Deng, M.; Li, H.; Li, M.; Zhang, C.; Shen, W.; Li, Y.; Guo, D.; Song, Y. Highly Reproducible SERS Arrays Directly Written by Inkjet Printing. *Nanoscale* **2015**, 7, 421-425.

(20) Wang, L.; Li, F.; Kuang, M.; Gao, M.; Wang, J.; Huang, Y.; Jiang, L.; Song, Y. Interface Manipulation for Printing Three-Dimensional Microstructures Under Magnetic Guiding. *small* **2015**, 11, 1900-1904.

(21) Bigioni, T.P.; Lin, X.-M.; Nguyen, T.T.; Corwin, E.I.; Witten, T.A.; Jaeger, H.M. Kinetically Driven Self Assembly of Highly Ordered Nanoparticle Monolayers. *Nat. Mater.* **2006**, 5, 265-270.

(22) Li, Y.; Yang, Q.; Li, M.; Song, Y. Rate-Dependent Interface Capture Beyond the Coffee-Ring Effect. *Sci. Rep.* **2016**, 6, 24628.

(23) Anyfantakis, M.; Geng, Z.; Morel, M.; Rudiuk, S.; Baigl, D. Modulation of the Coffee-Ring Effect in Particle/Surfactant Mixtures: the Importance of Particle–Interface Interactions. *Langmuir* **2015**, 31, 4113-4120.

(24) Mayarani, M.; Basavaraj, M.G.; Satapathy, D.K. Loosely Packed Monolayer Coffee Stains in Dried Drops of Soft Colloids. *Nanoscale* **2017**, 9, 18798-18803.

(25) Yunker, P.J.; Still, T.; Lohr, M.A.; Yodh, A. Suppression of the Coffee-Ring Effect by Shape-Dependent Capillary Interactions. *Nature* **2011**, 476, 308-311.

(26) Vermant, J. Fluid Mechanics: When Shape Matters. *Nature* **2011**, 476, 286-287.

(27) Tang, Y.; He, W.; Wang, S.; Tao, Z.; Cheng, L. The Superiority of Silver Nanoellipsoids Synthesized via a New Approach in Suppressing the Coffee-Ring Effect during Drying and Film Formation Processes. *Nanotechnology* **2014**, 25, 125602.

(28) Zhong, X.; Duan, F. Evaporation of Sessile Droplets Affected by Graphite Nanoparticles and Binary Base Fluids. *J. Phys. Chem. B* **2014**, 118, 13636-13645.

(29) Bhardwaj, R.; Fang, X.; Somasundaran, P.; Attinger, D. Self-Assembly of Colloidal Particles from Evaporating Droplets: Role of DLVO Interactions and Proposition of a Phase Diagram. *Langmuir* **2010**, 26, 7833-7842.

(30) Dugyala, V.R.; Basavaraj, M.G. Control over Coffee-Ring Formation in Evaporating Liquid Drops Containing Ellipsoids. *Langmuir* **2014**, 30, 8680-8686.

(31) Hu, H.; Larson, R.G. Marangoni Effect Reverses Coffee-Ring Depositions. *J. Phys. Chem. B* **2006**, 110, 7090-7094.

(32) Park, J.; Moon, J. Control of Colloidal Particle Deposit Patterns within Picoliter Droplets Ejected by Ink-Jet Printing. *Langmuir* **2006**, 22, 3506-3513.

(33) Majumder, M.; Rendall, C.S.; Eukel, J.A.; Wang, J.Y.; Behabtu, N.; Pint, C.L.; Liu, T.-Y.; Orbaek, A.W.; Mirri, F.; Nam, J.; Barron, A.R.; Hauge, R.H.; Schmidt, H.K.; Pasquali, M. Overcoming the “Coffee-Stain” Effect by Compositional Marangoni-Flow-Assisted Drop-Drying. *J. Phys. Chem. B* **2012**, 116, 6536-6542.

(34) Kajiya, T.; Kobayashi, W.; Okuzono, T.; Doi, M. Controlling the Drying and Film Formation Processes of Polymer Solution Droplets with Addition of Small Amount of Surfactants. *J. Phys. Chem. B* **2009**, 113, 15460-15466.

(35) Still, T.; Yunker, P.J.; Yodh, A.G. Surfactant-Induced Marangoni Eddies Alter the Coffee-Rings of Evaporating Colloidal Drops. *Langmuir* **2012**, 28, 4984-4988.

(36) Kim, H.; Boulogne, F.; Um, E.; Jacobi, I.; Button, E.; Stone, H.A. Controlled uniform coating from the interplay of Marangoni flows and surface-adsorbed macromolecules. *Phys. Rev. Lett.* **2016**, 116, 124501.

(37) Cui, L.; Zhang, J.; Zhang, X.; Huang, L.; Wang, Z.; Li, Y.; Gao, H.; Zhu, S.; Wang, T.; Yang, B. Suppression of the Coffee Ring Effect by Hydrosoluble Polymer Additives. *ACS Appl. Mater. Interfaces* **2012**, 4, 2775-2780.

(38) Deng, R.; Yang, L.; Bain, C.D. Combining Ink-Jet Printing with Emulsion Solvent-Evaporation to Pattern Polymeric Particles. *ACS Appl. Mater. Interfaces* **2018**, 10 (15), 12317-12322

(39) Yan, Q.; Gao, L.; Sharma, V.; Chiang, Y.-M.; Wong, C. Particle and Substrate Charge Effects on Colloidal Self-Assembly in a Sessile Drop. *Langmuir* **2008**, 24, 11518-11522.

(40) Banerjee, A.; Williams, I.; Azevedo, R.N.; Helgeson, M.E.; Squires, T.M. Soluto-Inertial Phenomena: Designing Long-Range, Long-Lasting, Surface-Specific Interactions in Suspensions. *Proc. Natl. Acad. Sci.* **2016**, 113, 8612-8617.

(41) Shi, N.; Nery-Azevedo, R.; Abdel-Fattah, A.I.; Squires, T.M. Diffusiophoretic Focusing of Suspended Colloids. *Phys. Rev. Lett.* 2016, 117, 258001.

(42) Talbot, E.; Berson, A.; Yang, L.; C.D. Bain. Internal Flows and Particle Transport inside Picoliter Droplets of Binary Solvent Mixtures. *Int'l Conf. Digital Printing Tech*. **2013**, 307-312.

(43) Talbot, E.; Berson, A.; Bain, C.D. Drying and Deposition of Picolitre Droplets of Colloidal Suspensions in Binary Solvent Mixtures. *Int'l Conf. Digital Printing Tech*. **2012**, 420-423.

(44) Barthel, H. Surface Interactions of Dimethylsiloxy Group-Modified Fumed Silica. *Colloids Surf. A* **1995**, 101, 217-226.

(45) Raghavan, S.R.; Hou, J.; Baker, G.L.; Khan, S.A. Colloidal Interactions Between Particles with Tethered Nonpolar Chains Dispersed in Polar Media: Direct Correlation between Dynamic Rheology and Interaction Parameters. *Langmuir* **2000**, 16, 1066-1077.

(46) Yow, H.N.; Biggs, S. Probing the Stability of Sterically Stabilized Polystyrene Particles by Centrifugal Sedimentation. *Soft Matter* **2013**, 9, 10031-10041.

(47) Blair, D.; Dufresne, E. *The Matlab Particle Tracking Code Repository, http://site.physics.georgetown.edu/matlab/. [Accessed 1 May 2018]*.

(48) Talbot, E. *Drying Inkjet Droplets-Internal Flows and Deposit Structure.* PhD thesis, Durham University 2014.

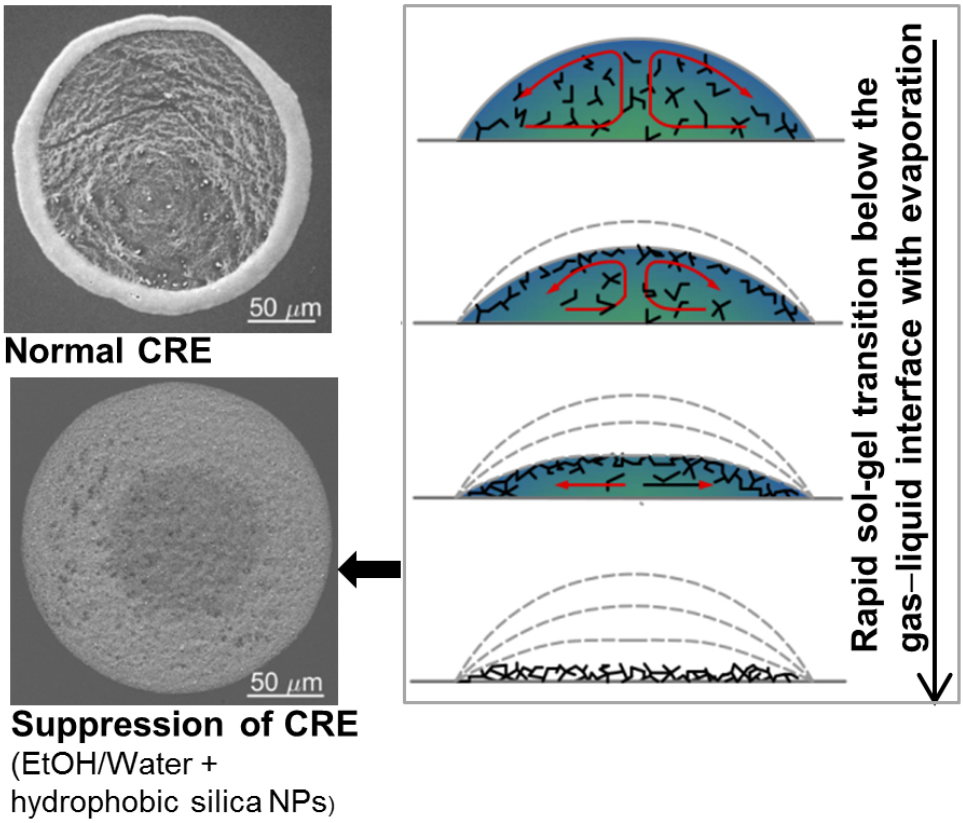

Table of Contents / Abstract Graphic

78x65mm (300 x 300 DPI)

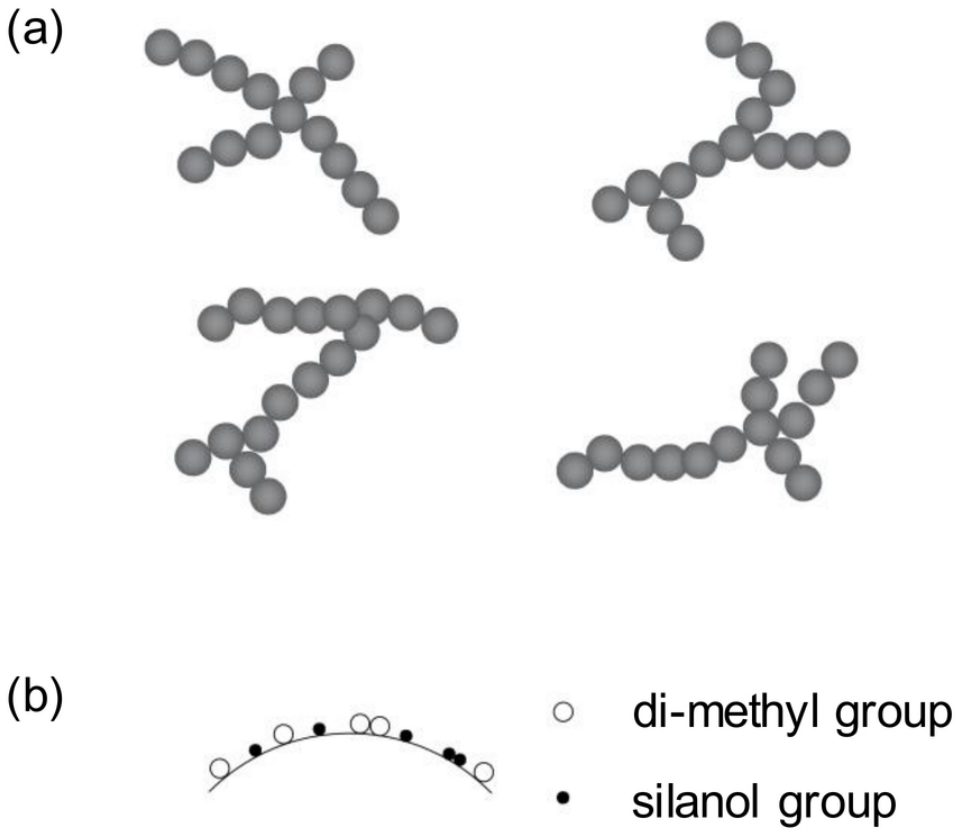

Figure 1. Schematic representation of primary structures of fumed silica (a) and the fumed silica surface (b).

75x63mm (300 x 300 DPI)

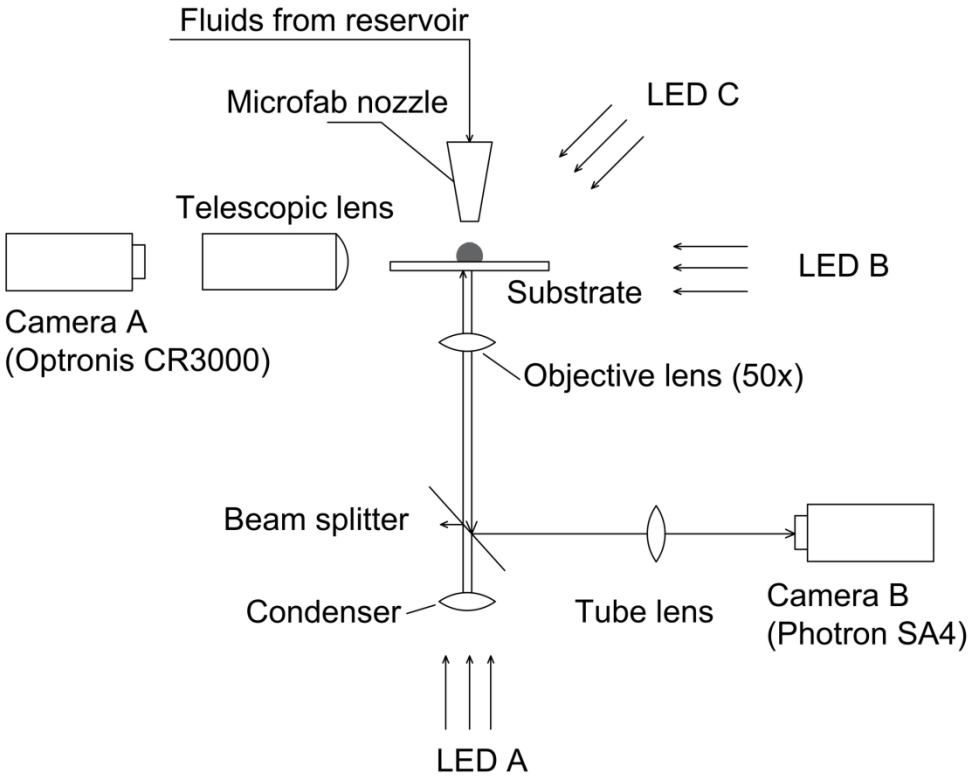

Figure 2. Schematic of the printing rig.

182x149mm (300 x 300 DPI)

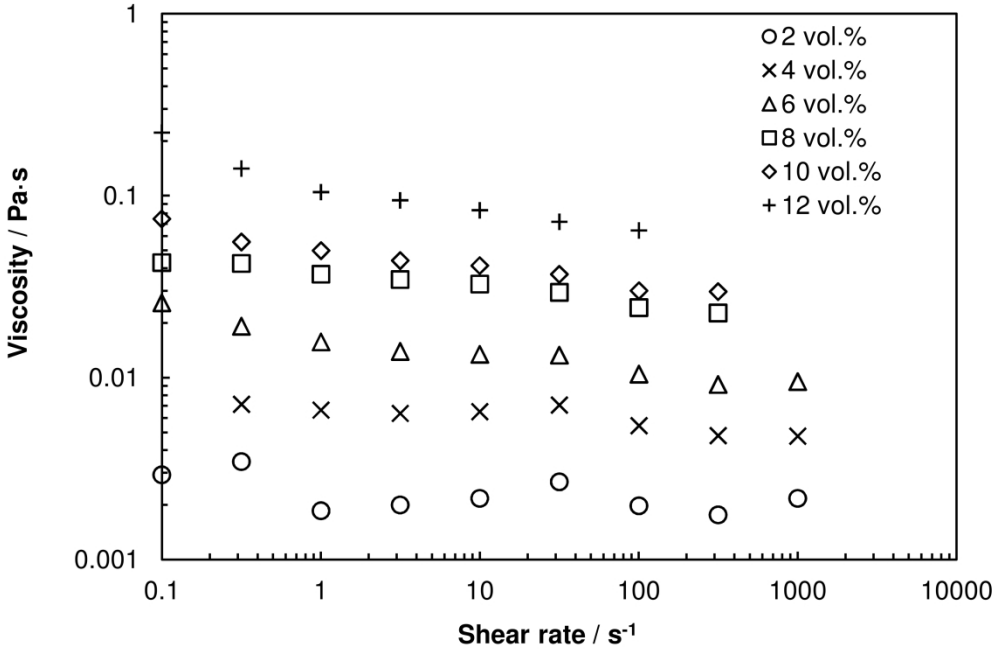

Figure 3. Steady-shear viscosity as a function of shear rate for ethanol containing different

166x110mm (600 x 600 DPI)

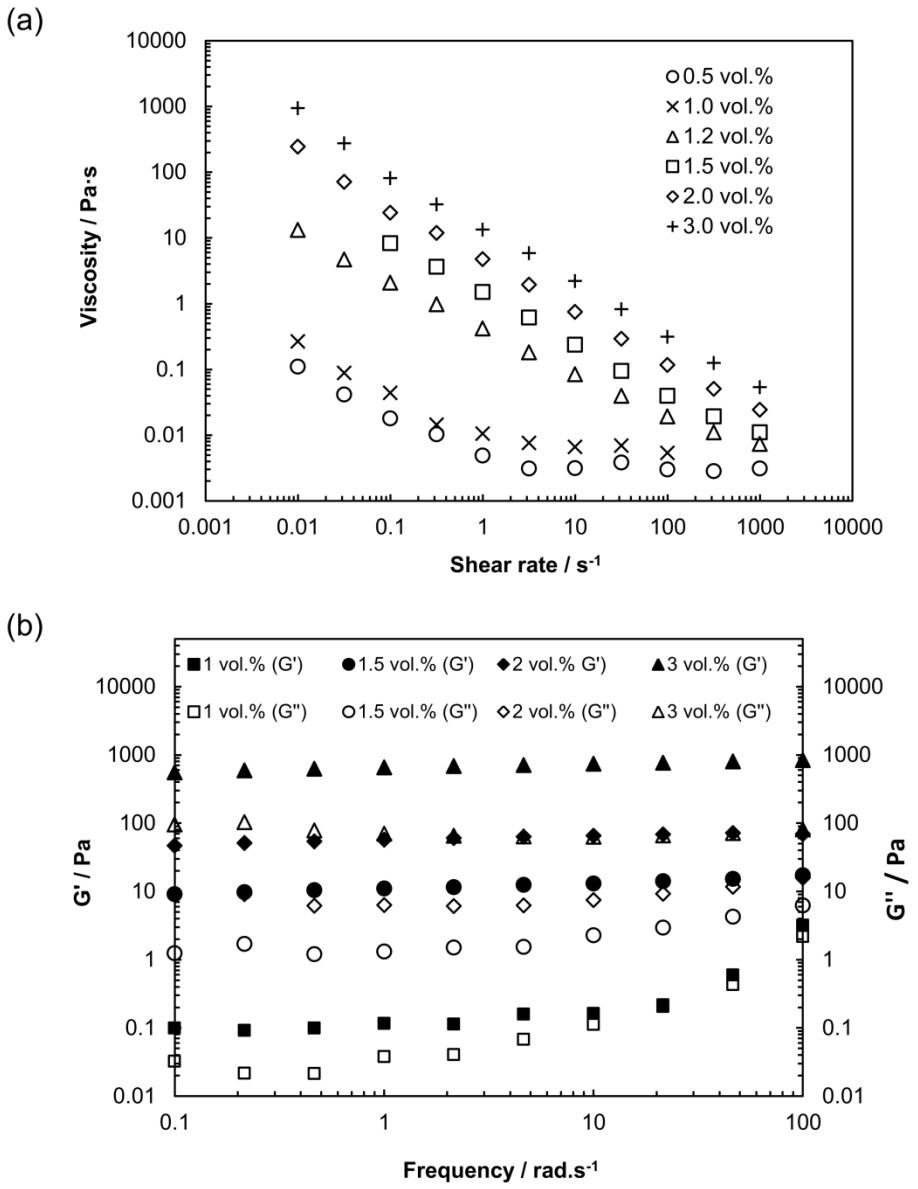

Figure 4. Rheology of 50 vol.% ethanol/water mixtures containing different concentrations of hydrophobic silica NPs.(a) steady-shear viscosity as a function of shear rate; (b) elastic moduli (G') and loss moduli (G'') as a function of frequency from oscillating shear rheology.

117x153mm (600 x 600 DPI)

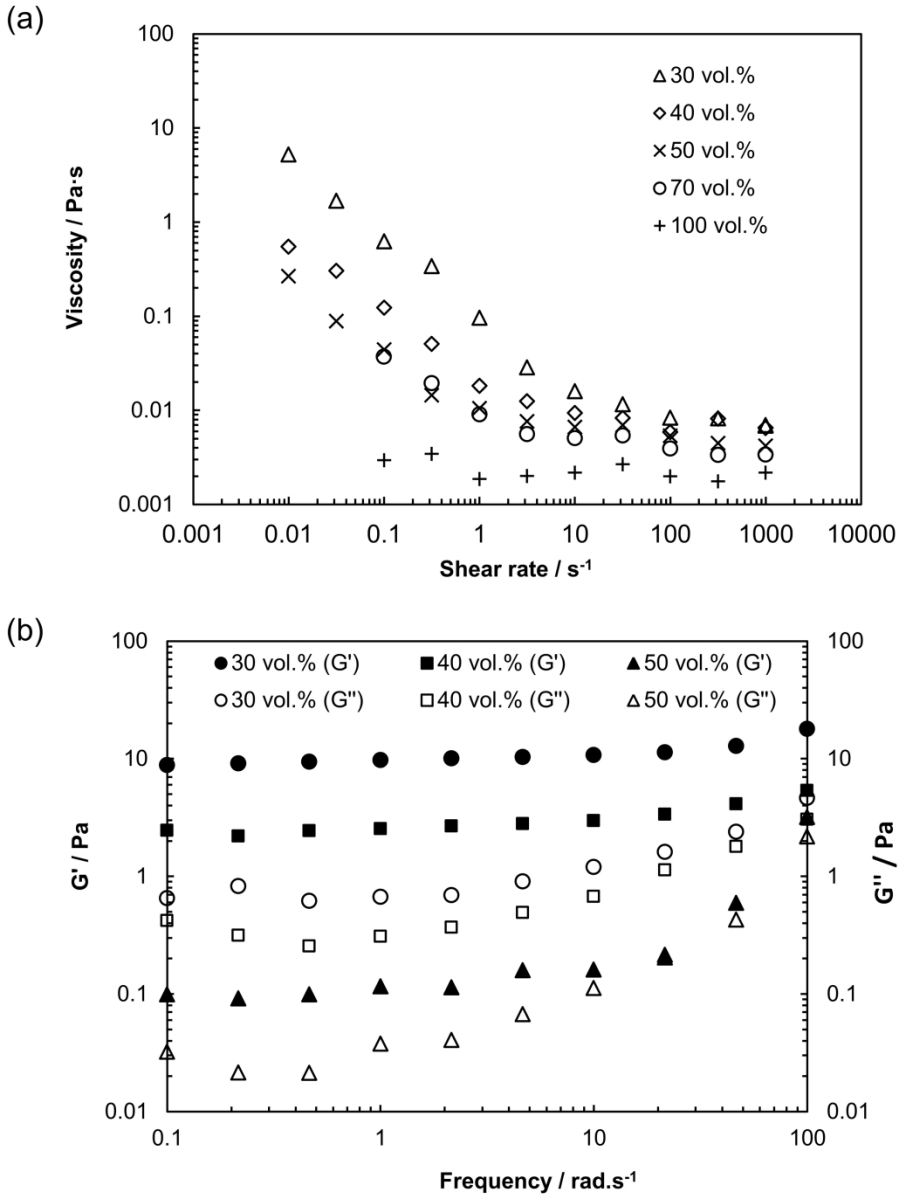

Figure 5. Rheology of ethanol/water mixtures with various ethanol concentrations and 1 vol.% hydrophobic silica NPs. (a) steady-shear viscosity as a function of shear rate; (b) elastic moduli (G') and loss moduli (G'') as a function of frequency from oscillating shear rheology.

114x151mm (600 x 600 DPI)

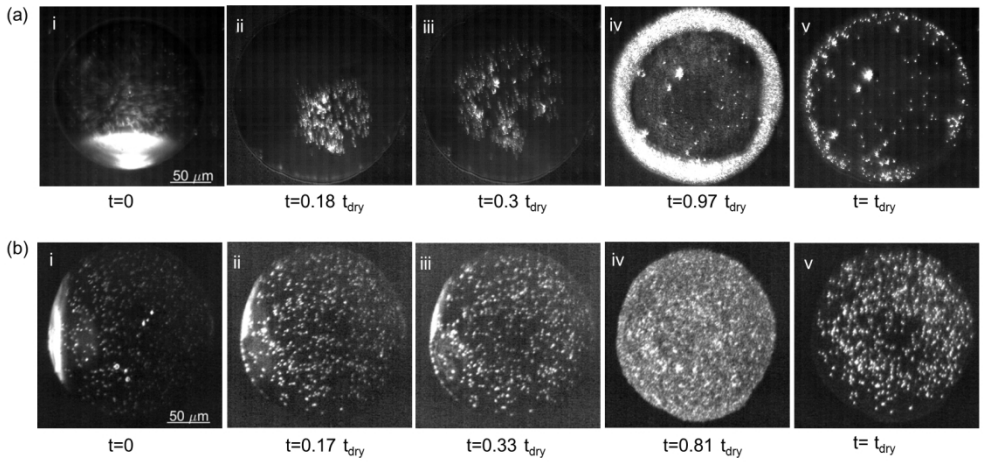

Figure 6. Dark-field images of a drying 50 vol.% ethanol/water droplet with 0.2 vol. % hydrophilic silica particles (a, t_{dry} = 4.6 s), and 0.2 vol.% hydrophobic silica particles (b, t_{dry} = 2.3 s). Both systems contain 0.01 vol.% PS tracer particles.

152x72mm (300 x 300 DPI)

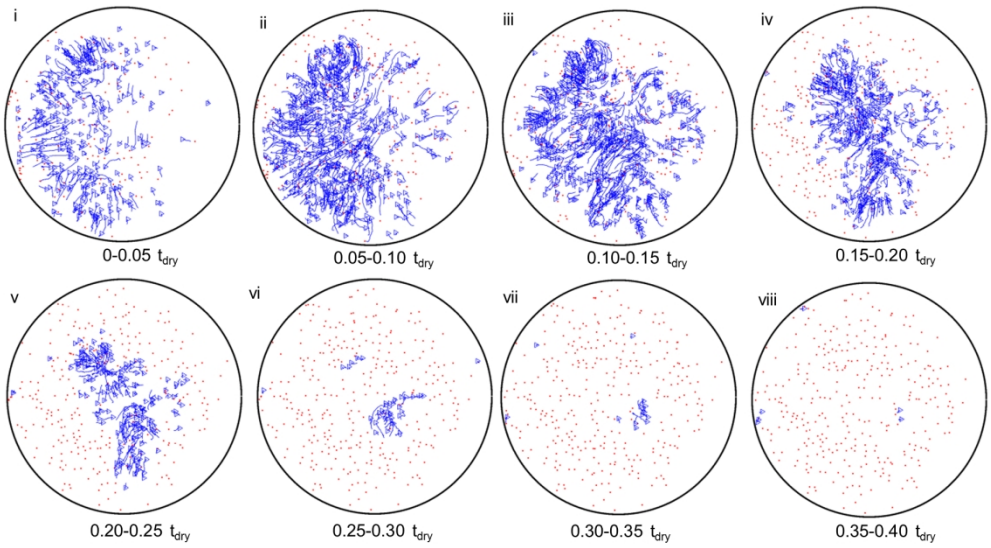

Figure 7. Tracer particle trajectories of a drying 50 vol.% ethanol/water droplet with 0.2 vol. % hydrophobic silica particles and 0.01 vol.% PS tracer particles. Refer to Figure 6b for the dark field images of the drying process. The red dots represent the stationary particles in the radial direction (movement < three pixels in the time interval). The blue lines represent the trajectories of moving particles, having a triangle at the end of the track to show the direction of motion.

161x88mm (300 x 300 DPI)

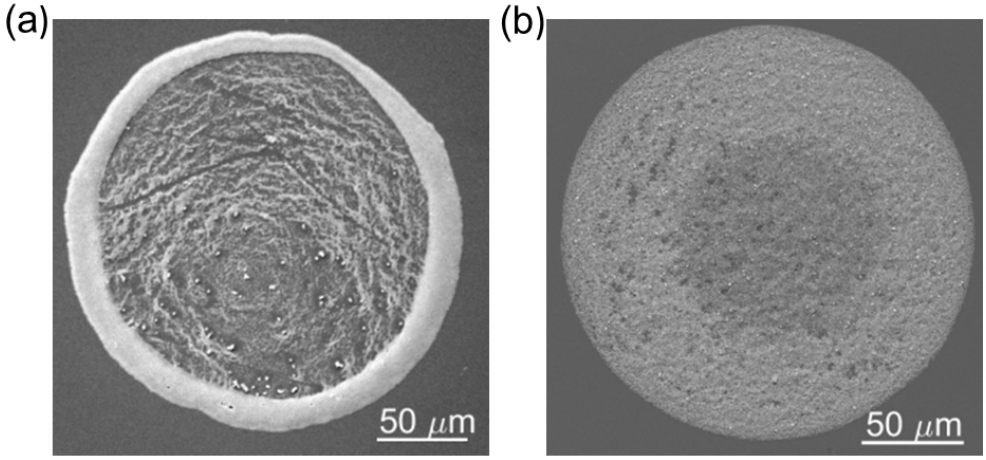

Figure 8. SEM images of deposits upon drying of a 50 vol.% ethanol/water droplet with 0.2 vol. % hydrophilic silica (a), and 0.2 vol.% hydrophobic silica (b). Both systems contain 0.01 vol.% PS tracer particles.

79x39mm (300 x 300 DPI)

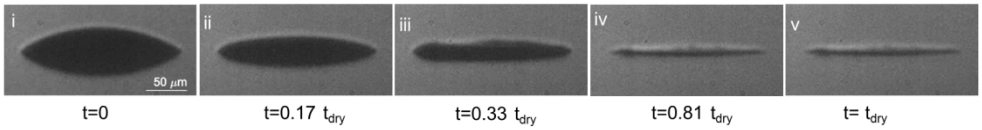

Figure 9. Side-view shadowgraph images of a drying 50 vol.% ethanol/water droplet with 0.2 vol.% hydrophobic silica particles and 0.01 vol.% PS tracer particles.

148x20mm (300 x 300 DPI)

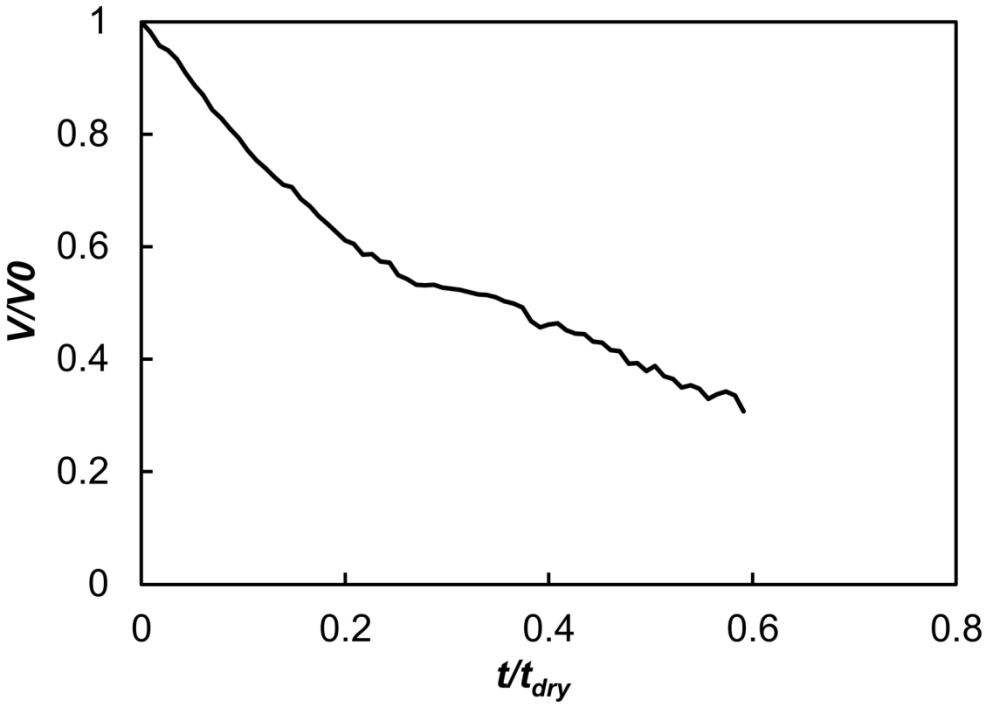

Figure 10. Volume profile with time for a drying 50 vol.% ethanol/water droplet with 0.2 vol.% hydrophobic silica particles and 0.01 vol.% PS tracer particles.

74x54mm (600 x 600 DPI)

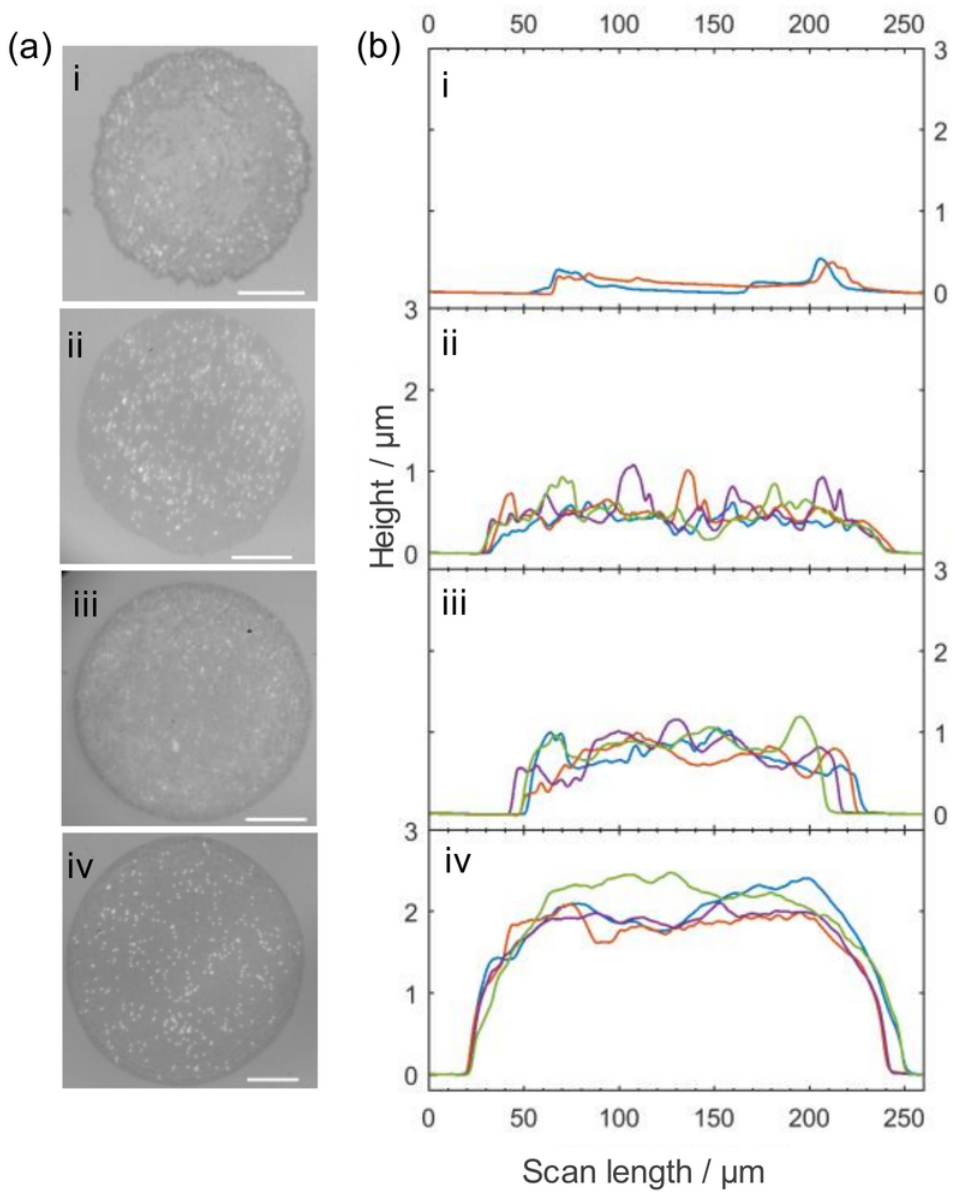

Figure 11. Reflection bright-field microscope images (a) and height profiles (b) of deposits upon drying of 50 vol.% ethanol/water droplets containing different concentrations of hydrophobic silica NPs: (i) 0.1 vol.%, (ii) 0.2 vol.%, (iii) 0.5 vol.%, (iv) 1 vol.%. All samples contained 0.01 vol.% PS tracer particles. The scale bars are 50 μm. Different coloured line profiles were measured from separate droplets dried under the same conditions.

69x84mm (300 x 300 DPI)

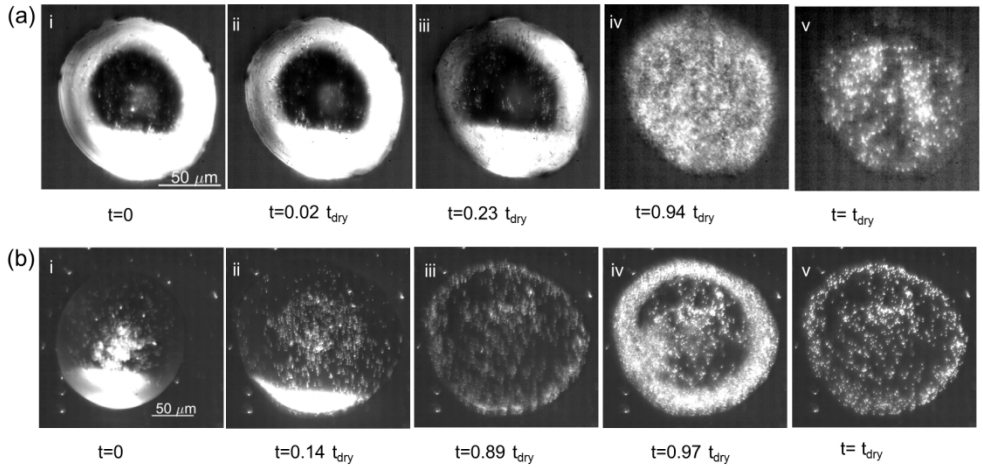

Figure 12. Dark-field images of a drying ethanol/water droplet with 0.2 vol.% hydrophobic silica particles and 0.01 vol.% PS tracer particles. (a) 10 vol.% ethanol/water; (b) 30 vol.% ethanol/water.

153x73mm (300 x 300 DPI)

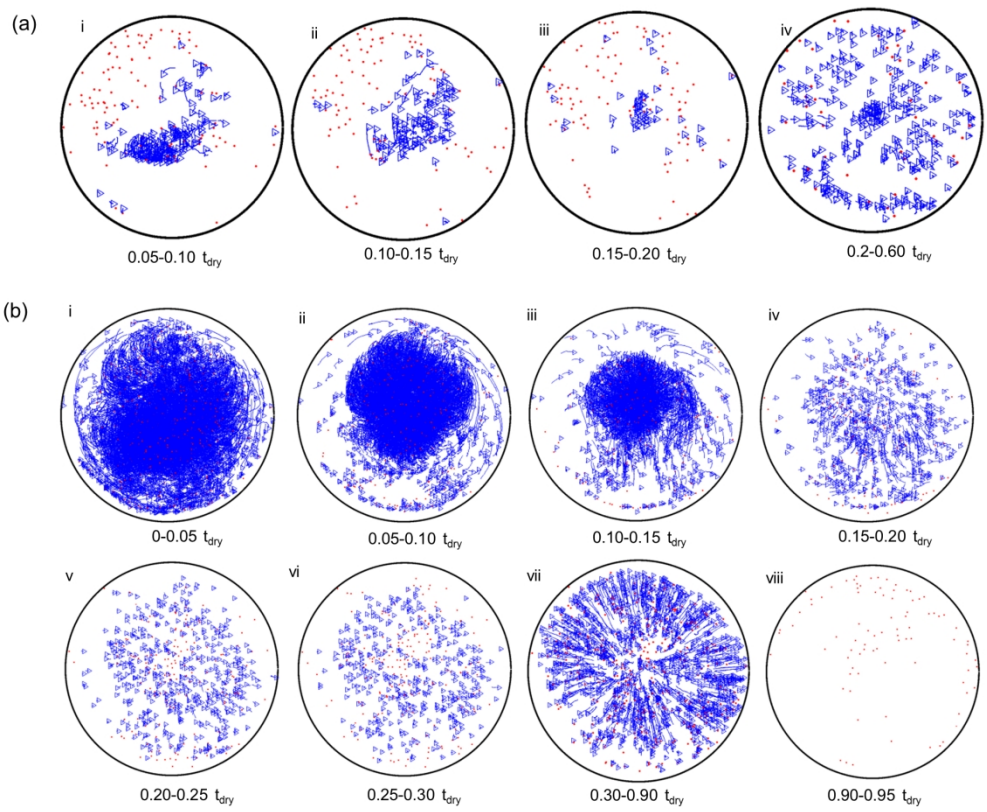

Figure 13. Particle trajectories of a drying ethanol/water droplet (a-10 vol.% ethanol/water; b-30 vol.% ethanol/water) with 0.2 vol. % hydrophobic silica particles and 0.01 vol.% PS tracer particles. Refer to Figure 12 for the dark field images of the drying process. The red dots represent the stationary particles in the radial direction (movement < three pixels in the time interval). The blue lines represent the trajectories of moving particles, having a triangle at the end of the track to show the direction of motion.

172x140mm (300 x 300 DPI)

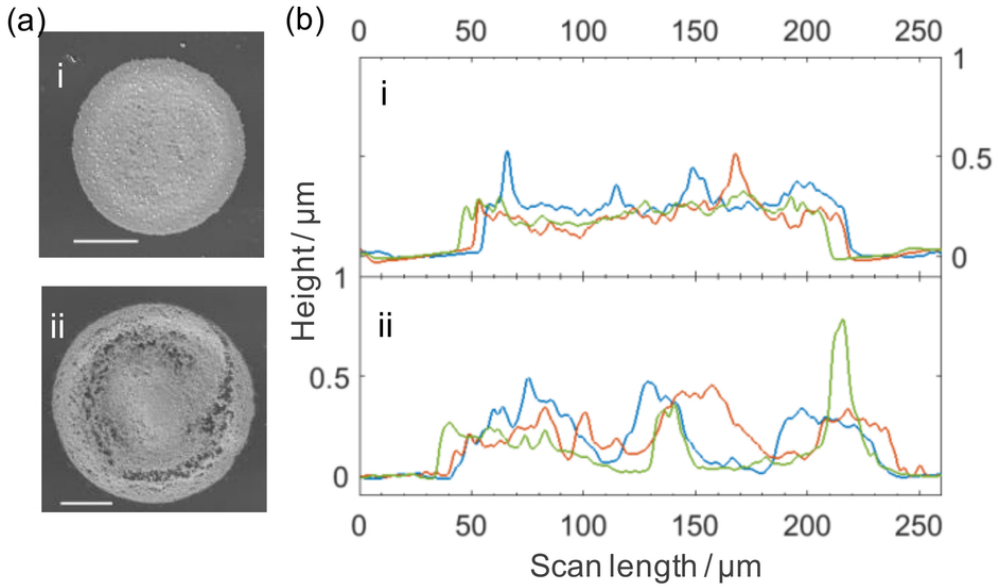

Figure 14. SEM images (a) and height profiles (b) of deposits upon drying of (i) 10 vol.% and (ii) 30 vol.% ethanol/water droplets containing 0.2 vol.% hydrophobic silica NPs and 0.01 vol.% PS tracer particles. The scale bars are 50 μm. Different coloured line profiles were measured from separate droplets dried under the same conditions.

79x47mm (300 x 300 DPI)

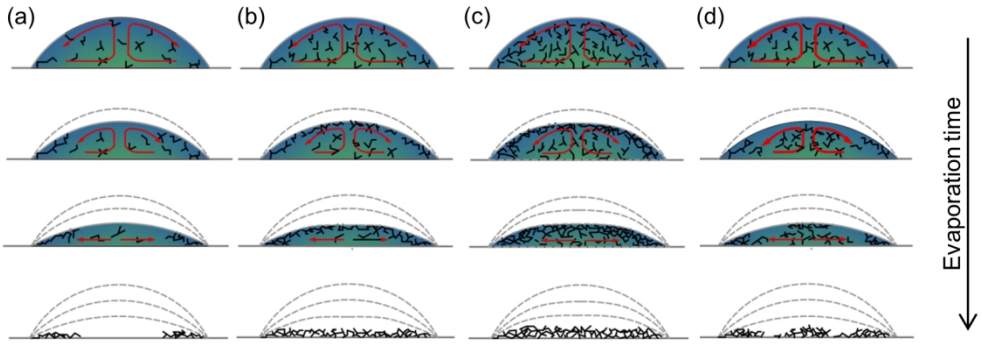

Figure 15. Illustrations of different drying patterns for ethanol/water droplets containing hydrophobic fumed silica. (a) – (c) are for drying of droplets in which Marangoni flow is moderate and (a) low silica concentration (0.1 vol%) where a sol–gel transition does not occur until late in the drying process, (b) medium silica concentration (0.2 vol%), (c) high silica concentration (0.5–1 vol%); (d) is for droplets with medium silica concentration in the presence of strong Marangoni flow (30 vol.% ethanol).

151x57mm (300 x 300 DPI)